

Gas Phase Chemistry in Dense Interstellar Clouds including Grain Surface Molecular Depletion and Desorption

E. A. Bergin,¹ W. D. Langer,² J. F. Goldsmith³

¹Five College Radio Astronomy Observatory, Department of Physics and Astronomy, University of Massachusetts, Amherst, MA 01003.

²Jet Propulsion Laboratory-California Institute of Technology, MS 169-506, Pasadena, CA, 91109

³National Astronomy and Ionosphere Center, Department of Astronomy, Cornell University, Ithaca, NY 14853-6801.

Abstract

We present time dependent models of the chemical evolution of molecular clouds which include depletion of atoms and molecules onto grain surfaces and desorption, as well as gas-phase interactions. We construct one-dimensional slab models to solve the abundances in the gas phase and on the grain surfaces as a function of extinction, density, and temperature. We include the major gas phase formation pathways for carbon-, oxygen-, and nitrogen-bearing species. To assess the effectiveness of different desorption mechanisms we have included three mechanisms to remove species from the grain mantle: thermal evaporation, cosmic ray spot heating, and direct photodesorption. A wide range of parameter space has been explored to examine the abundance of species present both on the grain mantle and in the gas phase as a function of both position in the cloud (visual extinction) and of evolutionary state (time).

Our pure gas phase model reproduces results similar to those derived in previous models of gas phase chemistry. However, the results of our models including depletion and desorption differ from those of previous models of gas-grain interactions in that molecules remain in the gas phase for times much greater than the depletion timescales. At these “(a)c” times the abundances of some simple species agree with abundances observed in the cold dark cloud TMC-1. The dominant mechanism that removes molecules from the grain mantles is cosmic ray desorption; this mechanism dominates over a wide range of conditions, $n(\text{H}_2) = 10^3 \text{ cm}^{-3}$ to 10^5 cm^{-3} , $T_{dust} < 20 \text{ K}$, and $\tau_V > 2 \text{ mag}$. Even though cosmic ray desorption preserves the gas phase chemistry at late times, molecules do show significant depletions from the gas phase. Examination of the dependence of depletion as a function of density shows that between densities $n(\text{H}_2) = 10^3 \text{ cm}^{-3}$ to 10^5 cm^{-3} several species including HCO^+ , HCN , and CN show gas phase abundance reductions of over an order of magnitude. Systematic comparisons of observed abundances in high density and low density regimes may provide evidence of these effects.

We present a history of grain mantle growth leading to several observationally relevant results. Our models predict that the grain mantles are dominated by CO, and at late times O₂, with only trace amounts of water ice. The CO:H₂O ratio in the grain mantle for our standard model is on the order of 10:1, in reasonable agreement with observations of non-polar CO ice features in ρ Ophiucus and Serpens. In addition, including only accretion from the gas phase without surface reactions cannot produce a grain mantle component dominated by H₂O as is commonly observed. We have also examined the interdependence of CO depletion with the space density of molecular hydrogen and binding energy to the grain surface and find that the observed depletion of CO in Taurus is inconsistent with CO bonding in an H₂O rich mantle. We suggest that if interstellar grains consist of an outer layer of CO ice then the binding energies for many species to the grain mantle may be lower than commonly used, and a significant portion of molecular material may be maintained in the gas phase.

1. Introduction

Over the past several decades many studies have been undertaken to examine the chemistry occurring in the dense molecular component of the interstellar medium (cf. Graedel, Langer, & Frerking 1982; Leung, Herbst, & Hill (1984); Millar and Freeman 1984; Herbst & Leung 1989; Langer & Graedel 1989). With the discovery of over 80 molecular species (Turner 1989) the study of chemical evolution in molecular clouds is of intrinsic interest. However, since the current state of knowledge of molecular clouds is basal for the most part (i.e. observations of the rotational and vibrational transitions of a variety of molecular species), knowledge of molecular formation processes is also necessary in order to interpret molecular observations of the ISM. Such basic quantities as the masses of clouds and densities, which are determined from observations of molecular emission lines, often require *a priori* knowledge of molecular abundances.

Chemical studies have concentrated almost exclusively on the pure gas phase ion-molecule chemistry and have been fairly successful in explaining the observed abundances of many molecules. However an important unknown is to what extent dust grains affect chemical processes. Dust grains are certainly important in shielding molecules in the interiors of molecular clouds from photodissociating radiation. In addition, the most abundant molecule in molecular clouds, H_2 , cannot be formed via gas phase processes and must be formed by hydrogen atoms recombining on grain surfaces (Hollenbach and Salpeter, 1977). Inclusion of grain accretion into chemical networks has shown that for typical cloud densities ($n(H_2) \sim 10^4 \text{ cm}^{-3}$) the timescale for molecular depletion is comparable to expected cloud ages. If molecules stick efficiently to grain mantles, all molecules should exist on the grain surfaces and not in the gas phase (Iglesias 1977).

One deterrent to including grain accretion and surface reactions in chemical models has been the paucity of direct observational evidence of molecules on grain surfaces.

Over the last few years, improved resolution and sensitivity of infrared spectrometers have allowed observations of solid state absorption lines, providing evidence that significant amounts of molecules such as H_2O and CO are frozen on grain surfaces towards dense protostellar cores and along lines of sight towards field stars obscured by dense molecular material. For a useful summary of the current state of observations of solid state features see Whittet (1993).

More recently, laboratory studies of solid state CO features combined with high resolution observations of CO ice towards young stars embedded in molecular clouds have revealed the presence of two independent spectral components along many lines of sight. These components, distinguished by the characteristics of the absorption profile, are suggested to be CO embedded in a mantle dominated by polar molecules (e.g. H_2O Sandford et al. 1988) and a mantle dominated by nonpolar molecules (Sandford et al. 1988; Tielens et al. 1991). There is little evidence for the components thought to comprise the nonpolar mantle since the main candidates O_2 , N_2 , and CO_2 are currently unobservable. The two grain mantle components may reflect differences in the grain mantle constituents along the line-of-sight or gas phase abundance differences at the time of mantle formation. The differences in the grain mantle may also depend on the processes which selectively remove particular species from the mantle. These observations suggest that the history of how and when molecules deplete onto grain mantles is very important, since it depends on what molecules are present in the gas phase at various times and on the efficiency of the desorption processes and to a significant degree may determine the final composition of both the gas phase and the grain mantle.

To extend our knowledge of the mantle formation further we have modeled gas phase chemical evolution including the effects of grain depletion and desorption in regions exposed to enhanced ultraviolet (UV) flux. There exists a considerable body of knowledge of the gas phase chemistry and evidence for the depletion of molecules onto the surfaces

of grains (cf. van Dishoeck et al 1993; Whittet 1993). In addition to measurements of grain surface abundances there is also a growing body of evidence concerning the erosion of grain mantles near sites of star formation. At star formation sites, such as the Orion hot core, high abundances of H_2O and other molecules indicate that mechanisms other than gas phase chemistry are operative (Plambeck and Wright 1987; Blake et al 1987). In this and other hot compact star forming regions the abundance of deuterated H_2O appears to be enhanced (Jacq et al 1990). The observed D/H ratios are consistent with formation at temperatures < 20 K, much less than the gas temperature, suggesting the deuterated molecules are the result of fractionation at low temperatures, "fossilized" on the surface of the grains, and returning to the gas phase as the dust grains warm up with the onset of star formation. In the case of deuterated formaldehyde, Turner (1990) has concluded from measurements of doubly deuterated formaldehyde, D_2CO , that grain surfaces must play an active role in the formation of this species.

The importance of understanding the effects of grains on chemistry is evident. Since the pioneering work of Salpeter and co-workers, several efforts have been directed in this regard. These have proposed complicated surface reaction networks and many different desorption mechanisms to remove molecules from the grain surfaces (for useful summaries see Williams 1993 and Herbst 1993). Many of the current theoretical efforts, such as the work by Hasegawa & Herbst (1993) and Hasegawa, Herbst, & Leung (1992), have concentrated on studying effects of grain surface chemistry on the chemical evolution of molecular clouds in dense well shielded regions. In this study we extend the theoretical models to the exterior regions of molecular clouds in addition to the dense well shielded interior. We model how molecular grain mantles evolve as a result of the competition between the processes of depletion and desorption, in order to examine the time history of which molecules are present on the mantle as a function of cloud depth (visual extinction). We also examine the sensitivity of the processes of depletion and

desorption upon changing physical conditions by varying the density, dust temperature, and UV flux.

In our models we have initially taken the somewhat restrictive view of not allowing reactions on the grain mantle since the addition of surface reactions adds additional complexity and uncertainty. The exclusion of surface reactions is certainly an approximation, since reactions on the surfaces of grains are thought to form molecular hydrogen, the most abundant species in molecular clouds (Hollenbach & Salpeter 1970). However, the observations of solid CO embedded in a nonpolar matrix provides some evidence of molecules that were directly deposited on the grains from the gas phase and not created by surface processes (Tielens et al 1991; Whittet 1993). We intend to include a surface reaction network in future models.

In section 2 we present the chemical model that is used to examine the gas-grain interactions. Section 3 presents the results from the chemical model examining both the time dependence of the chemistry and the dependence of the chemistry on optical depth. Section 4 contains a detailed discussion of the results applied to observations of both gas phase abundances and grain surface abundances. Section 5 presents a brief summary of the results.

2. Chemical Model

2.1. Gas Phase Chemistry

The chemical reaction network for gas phase reactions consists of the major formation and destruction pathways for carbon-, oxygen-, and nitrogen-bearing species. The reaction set links 82 species through a network of 1072 reactions first compiled by Viala (1986) and later updated by Benayoun, Nercessian, & Viala (1991). Since we are mod-

Along both the edges of clouds and interior regions the chemical reaction scheme includes the photodissociation and photoionization of molecules. The transition from atomic to molecular form for most molecular species occurs much deeper in the cloud than that for H I to H_2 . Therefore we have not included the effects of H_2 self-shielding. In our model the molecular hydrogen density remains constant in time. The main destruction process for H_2 is cosmic ray ionization ($\zeta = 2.0 \times 10^{-17} \text{ s}^{-1}$) and the main formation path is immediate H_2 formation when a hydrogen atom sticks to a grain. It should be kept in mind, however, that for very small values of visual extinction (< 0.25 – 0.5 mag) the amount of H_2 will be overestimated. We have made several changes in the Viala reaction network to bring it up to date, which we describe in Appendix A.

2.2. Gas-Grain Interactions

2.2.1. Depletion and Binding

The rate of deposition of a molecule in the gas phase onto a grain surface is

$$k_{dep} = \pi a^2 \bar{v} S n_{gr} \quad (\text{s}^{-1}). \quad (1)$$

where a is the grain radius, \bar{v} is the mean thermal velocity, S is the sticking coefficient, and n_{gr} the space density of grains. We have used “classical” grains of radius 1000 \AA and space density $n_{gr} = 1.3 \times 10^{-21} \text{ cm}^{-3}$. We have assumed a sticking coefficient of 1.0 for all neutral atoms and molecules except atomic and molecular hydrogen. Due to its weak binding, H_2 is not expected to be depleted onto interstellar grains (Sandford & Allamandola, 1992); hence we adopt a sticking coefficient of zero. For atomic hydrogen we have adopted $S = 0.1$, motivated by theoretical calculations of sticking coefficients by Leitch-Devlin & Williams (1985).

Because of the high thermal velocity of electrons compared to positive ions, grains throughout most of the interstellar clouds (except near the edge where UV photoelectron ejection keeps grains positively charged) are expected to be negatively charged (Spitzer 1978). d'Hendecourt, Allamandola, & Greenberg (1985) presented a treatment of the maximum charge accumulated by an interstellar grain. They concluded that under the cold conditions in dense well shielded regions of molecular clouds a grain with a radius of 1000 Å will have a maximum charge of 1 e. Thus in our treatment we have assumed a grain charge of one electron per grain. Upon collision with a grain we assume a positive ion will undergo dissociative recombination with the same branching ratios as in the gas phase. In this fashion $\text{HCO}^+ + (\text{grain})^- \rightarrow \text{H} + \text{CO}$. After the positive ion is neutralized, an electron is assumed to immediately stick to the grain surface replenishing its charge.

Once the neutral species sticks to the grain surface it becomes bound. It is commonly thought that most molecules are weakly adsorbed or physisorbed onto the surfaces of interstellar grains with binding energies $E_b \sim 0.1$ eV or 1000 K (Williams, 1968; Watson & Salpeter 1972). This assumption is not always correct, since some molecules may chemically bind to the surfaces (chemisorption) with consequent higher values of E_b , typically ~ 2 eV (Tielens & Allamandola 1987). An example is the hydrogen bonding in H_2O ice where the binding energy has been measured to be $E_b > 4800$ K (Sandford & Allamandola 1988). We have adopted the binding energy scheme of Hasegawa, Herbst & Leung (1992 [11111,]) who assumed that all molecules are physisorbed onto the surfaces of grains. The values used by HHL were extracted from previous studies performed by Allen & Robinson (1977) and Tielens & Allamandola (1987). In particular, 11111, assumed that molecules bind to a silicon dioxide surface and atoms bind to an icy surface (see Table 1 from HHL). The values chosen for binding energies are highly uncertain, since few have been measured in the laboratory and the binding surface may change as grains evolve. The choice of E_b is critical since the desorption processes are highly dependent on the

binding energy. We will address the consequences of these assumptions in the following sections.

2.2.2. Desorption

One of the more uncertain aspects of modeling gas-grain chemical interactions is determining the dominant mechanism that removes species from the mantles. Several studies have been performed, proposing many different desorption mechanisms (cf. Leger, Jura, & Omont 1985, and Schutte & Greenberg 1991). To assess the effectiveness of different desorption mechanisms throughout the cloud, we have included three potentially important desorption mechanisms: thermal evaporation, cosmic ray induced heating, and direct photodesorption.

The rate for direct thermal evaporation or sublimation is given by

$$k_{evap} = \nu_0 \exp(-E_b(X)/kT_{dust}) \text{ (s}^{-1}\text{)} \quad (2)$$

where $E_b(X)$ is the binding energy of the adsorbed species X, ν_0 is the lattice vibration frequency for the adsorbed atom or molecule, k is the Boltzmann constant, and T_{dust} is the temperature of the dust grain. The lattice vibration frequency is expressed as

$$\nu_0 = \sqrt{\frac{2n_s E_b(X)}{\pi^2 m}} \text{ (s}^{-1}\text{)} \quad (3)$$

where m is the mass of the adsorbed species, n_s is the surface density of sites, $n_s = 1.5 \times 10^{15} \text{ cm}^{-2}$ (Tielens & Allamandola 1987). At typical dust temperatures for dense regions of molecular clouds, ($T_{dust} = 10\text{--}30 \text{ K}$) the timescale for thermal evaporation is generally much greater than typical cloud lifetimes. However, for high dust temperatures or low values of the binding energy, thermal evaporation of molecules is not negligible.

Watson & Salpeter (1972) first proposed that energetic nuclei might eject molecules from grain mantles either by raising the temperature of the entire grain or by spot heating near the impact site. This process was re-examined by Leger et al (1985) who found that for grain radius $a > 25 \mu\text{m}$, cosmic ray spot heating is important (for smaller grains the whole grain is heated). Because the energy deposition is proportional to the square of the atomic number, cosmic ray heating is dominated by the rarer heavy ions (Watson & Salpeter 1972; Leger et al 1985). Recently Hasegawa & Herbst (1993 [1111]) rendered the results of Leger et al (1985) for cosmic ray spot heating and subsequent thermal evaporation into a more manageable form and we have adopted their formulation.

[1111] assumed that after impact of a relativistic Fe nucleus the grain temperature quickly reaches a peak value of $\sim 70 \text{ K}$, and then drops predominantly via thermal evaporation of volatile species. Since thermal evaporation is a strong function of the grain temperature, most of the volatile species will evaporate at or near the peak temperature. The grain temperature is therefore assumed to be near 70 K directly after a heating episode, and well below this temperature otherwise. [1111] express the cosmic ray desorption rate for a particular species as the product of the fraction of time spent near 70 K and the evaporative cooling rate for a given atom or molecule at 70 K , or

$$k_{cr} \approx f(70K)k_{ev}(P_b(X), T_{dust} = 70K) s^{-1} \quad (4)$$

where $f(70 \text{ K})$, the fraction of time spent near 70 K is defined as the ratio of the timescale for cooling via thermal evaporation of volatiles to the time interval between successive heatings and is $\sim 3.16 \times 10^{-19}$. This parameterization is certainly an approximation to cosmic ray desorption, since the derivation requires significant volatile species present as a cooling mechanism for the mantle, which is not the case at early times in our models. However, given the uncertainties in the binding energies, we believe that these

rates allow at a least first order attempt to study the effects of depletion and cosmic ray desorption.

Photodesorption of a physisorbed or chemisorbed molecule on a grain may occur in several distinct fashions. The first is direct absorption of a UV photon by an adsorbed molecule which puts an electron in an excited state. If the interaction between the excited state is repulsive with the binding surface then the excited molecule may be ejected from the surface (Watson & Salpeter 1972). The rate for direct photodesorption as given by d'Hendecourt et al (1985) is

$$k_{pd} = Y\chi\exp(-2A_v)\pi a^2 s^{-1} \quad (5)$$

where Y is the photodesorption yield (number of molecules desorbed per incident photon), and χ is the UV field enhancement factor in units of the mean interstellar UV field (Habing, 1968). The exponential term accounts for the attenuation of the ultraviolet field. The efficiency of this process is quite uncertain. Measurements of photodesorption yields have been performed by Greenberg (1973) in the wavelength range 2000 to 2750 Å and found to be in the range $10^{-5} - 10^{-1}$. However, the molecules used in the experiment did not have strong absorption bands in the wavelength region studied. Additional measurements by Bourdon, Prince & Duley (1982) suggest significantly lower yields on the order of 10^0 ; these experiments studied only strongly physisorbed species over the wavelength region of 4500 to 6000 Å, well outside of the ultraviolet portion of the spectrum.

Other methods of photodesorption rely on indirect ways to remove an adsorbed species. One such method is absorption of a photon by the bonding surface, thus breaking a relative high energy chemisorption bond and leaving the molecule in a relatively weaker physisorbed state where it is susceptible to evaporation (Draine & Salpeter 1979).

In another indirect photodesorption process, a photon dissociates a molecule absorbed inside the lattice, as proposed by Hartquist & Williams (1991) and Willacy & Williams (1993) for H₂O ice. An ultraviolet photon absorbed by the water ice will dissociate H₂O → OH + H with an estimated yield of 0.1 per ultraviolet photon. The hydrogen atom will carry off most of the dissociation energy and create a hot spot where evaporation of weakly adsorbed species will be enhanced.

The efficiencies of these processes are not well understood. For yields < 10⁻⁵ photodesorption is relatively unimportant in our models. However laboratory measurements at shorter wavelengths and for species abundant in molecular clouds have not been made. Extrapolation to ultraviolet wavelengths (Greenberg 1973) suggest that yields as high as 10⁻² might be appropriate. To assess the importance of direct photodesorption we have adopted a yield of 10⁻⁴, a value higher than measured in the laboratory. To further assess the importance and maximum contribution of photodesorption, as well as indirect photodesorption, we have also examined the effects of yields > 10⁻⁴.

2.3. One Dimensional Chemical Model

The coupled differential equations governing the gas-grain chemical evolution were solved using a variant of the Gear (1971) algorithm: LSODE (Hindmarsh 1980). This code, which is a linear implicit multistep method, utilized variable time step and error control techniques to preserve numerical accuracy during the integration. The adjustable variables for a given calculation are the space density of *molecular* hydrogen, $n(\text{H}_2)$, the factor by which the UV radiation is enhanced, χ , the gas temperature, T_{gas} , the dust temperature, T_{dust} , and the visual extinction to the center of the cloud, A_V . τ_V is the visual extinction proceeding from edge to center such that $\tau_V^{max} = A_V$.

A one dimensional cloud model was constructed by running a pseudo-time dependent

calculation up to 10^7 yr with fixed physical conditions for a given visual extinction, defining a “zone”. The visual extinction was then incremented from the cloud edge ($\tau_V = 0.0$ mag) up to some maximum value, normally $A_V \sim 10.0$ mag, defining a set of zones. A typical run had 30 zones between $\tau_V \sim 0.0$ - 10.0 mag. Each zone was independent of other zones except for the calculation of total CO and H₂ column densities required for the CO self-shielding photorate (see Appendix A). In this fashion the physical conditions $n(\text{H}_2)$, T_{gas} , and T_{dust} can be expressed as functions of the visual extinction or be kept constant for a “uniform” cloud model.

For the initial conditions we use depleted elemental abundances based for the most part on observations in the diffuse cloud towards ζ Ophiuchi (Savage, Cardelli, and Sofia 1992, see also Graedel et al 1982). These abundances, listed in Table 1, represent moderate depletions (~ 0.2) for C, N, O, while the heavier metals are significantly depleted. The carbon, sulfur, silicon, and iron are assumed to be initially all in ionized form while oxygen and nitrogen are neutral. These initial abundances are similar to the ones used by IIII and III in models with their “normal” initial conditions.

3. Results

The one dimensional model of gas phase chemistry including grain depletion and desorption was run for a single cloud model, labeled the standard model, where physical parameters were kept constant throughout the cloud. The model was also run over a range of values of $n(\text{H}_2)$, T_{dust} , and χ to study the effects of changing physical conditions on the chemistry, which are presented in Appendix 11. The physical conditions of the standard model are $n(\text{H}_2) = 10^4 \text{ cm}^{-3}$, $T_{gas} = 20 \text{ K}$, $T_{dust} = 10 \text{ K}$, and $\chi = 1.0$. The calculations included all desorption processes presented in Section 2.2.2 unless otherwise noted. These are representative values for physical conditions inside molecular clouds

and provide a base from which to examine differences.

3.1. Time Dependence

To show the limiting case of total depletion we performed one calculation of standard model without cosmic ray desorption, similar to the results presented by Iglesias (1977) and Brown & Charnley (1990). This is presented in Figure 1 for deep in the cloud ($\tau_V = 10.3$ mag) where photoprocesses can be neglected. Thermal evaporation is therefore the only relevant desorption mechanism. Since at $T_{dust} = 10$ K the timescale for thermal evaporation is much greater than the depletion timescales, all molecules are seen to disappear from the gas phase at the characteristic depletion time of $\sim 10^6$ years. These results remain essentially unchanged for T_{dust} up to ~ 20 K. A characteristic of most ion-molecule models in the gas phase is that O_2 and N_2 peak in the gas phase at much later times than CO which quickly locks up most of the carbon (Graedel et al 1982, Langer and Graedel 1989). *Thus, the mantle composition reflects the gas phase abundances at earlier times and is dominated by atomic oxygen and CO. H_2O remains a trace species in the mantle where its fractional abundance remains below 10^{-7} .* As found by Brown, Charnley, & Millar (1988a) and Brown & Charnley (1990) the abundances of some highly reactive radicals, such as OH do show abundance enhancements (above normal gas phase evolution without grain depletion) prior to the onset of depletion at 10^6 yr. For OH in particular this is a result of a decrease in its destruction rate due to depletion of molecular oxygen. In this example, the depletion timescales are proportional to the density. Therefore rapid depletion of atoms and molecules prior to 10^6 yr requires $n(H_2) > 10^5$ cm^{-3} .

Our standard model includes all desorption processes and these modify the time dependent evolution significantly. The results are shown in Figure 2 for species which represent the dominant reservoirs of carbon, oxygen, and nitrogen in the interior ($\tau_V =$

10.3 mag) and near the edge of the cloud ($\tau_V = 2.1$ mag). *The most striking feature in Figure 2, is that deep in the cloud ($\tau_V = 10.3$ mag.), the molecules, including highly polar H_2O , remain in the gas phase despite the high depletion role.* This is in contrast to Figure 1 that indicated that all molecules disappear from the gas phase after $\simeq 10^6$ yr. The persistence of molecules in the gas phase at all times is due to cosmic ray desorption (discussed in section 2.2.2). The grain surface composition has been highly modified by the cosmic rays, which quickly remove the weakly bound atoms and allow formation of molecular oxygen and nitrogen in the gas phase. These species subsequently deplete onto the grain surface. Hence the composition of the molecular grain mantle is dominated by O_2 and CO , in contrast to the case excluding cosmic ray desorption where O and CO are the most abundant species present in the mantle. The quick release of atoms from the grain surface also removes the effects of abundance enhancements of reactive radicals (e.g. OH) so that the chemistry evolves in a manner similar to the early time pure gas phase. In general, radicals do show abundance enhancements over the pure gas phase results, but only by at most a factor of two. At later times the gas phase abundances are heavily depleted and predominantly in molecular form.

We can examine these effects for various species more closely by comparing the timescales for depletion and desorption listed in Table 2. Since the timescales for cosmic ray desorption are highly dependent on the binding energy there exists a wide range of values: the strongly bound water molecule shows the cosmic ray desorption timescale, $t_{cr} > t_{dep}$, the depletion timescale. The intermediate binding of CO exhibits $t_{cr} \approx t_{dep}$, while the weakly bound carbon atom has $t_{cr} < t_{dep}$. In our model, the gas phase chemistry is strongly influenced by the desorption of atoms from the surface. *Since atoms have low binding energies, cosmic ray desorption rapidly removes the atoms from the surface allowing an active gas phase chemistry to continue for very long times.* In the work by Hasegawa & Herbst (1993) this effect is absent because the atoms are assumed

to undergo rapid catalytic reactions on the grain surfaces processing them to molecules which have higher binding energies. In the present paper we have omitted catalytic reactions in order to understand the interdependence of the gas phase chemistry and the gas phase deposition upon the chemical evolution in molecular clouds including a desorption model.

The lower panel in Figure 2 shows the chemical evolution at $\tau_V \sim 2$ mag, where photoprocesses play a more important role. However, even at low extinctions, the process of cosmic ray desorption dominates over photodesorption. As an example for CO $t_{cr} = 2.2 \times 10^6$ yr is less than the photodesorption timescale (at $\tau_V = 2.1$ mag) of 6.0×10^7 yr. The important mechanism at low extinctions is not photodesorption but photodestruction which suppresses the formation of molecules such as O₂ and N₂, keeping the oxygen and nitrogen in atomic form. Cosmic ray grain surface desorption then maintains O and N in the gas phase, leaving the strongly self-shielded CO molecule and trace amounts of O, N₂ and H₂CO on the grain mantles. Thus there are some significant differences in both the gas phase and the mantle composition between $\tau_V = 2.1$ and 10.3 mag, which will be examined in the following section.

Thus far we have restricted our discussion to only the dominant reservoirs of carbon, oxygen, and nitrogen. In Figures 3 and 4 we present the standard model for other species which are observationally important. Figure 3 shows the evolution of the carbon and oxygen species: C₂H, C₂H₂, CO₂, H₂CO, and HCO⁺. Examining the upper panel which is representative of a well shielded region, at early times ($< 10^5$ yr) these molecules exhibit a very rich chemistry in spite of the inclusion of grain depletion. Since the removal of atomic carbon from the gas phase is inefficient, species which are chemically linked to C, such as C₂H and C₂H₂, show a dependence at early times similar to models which do not contain depletion (Leung, Herbst & Huebner 1984). The rapid drop in abundance of C₂H, C₂H₂, and H₂CO at 7×10^5 yr is related to the sharp drop in the

neutral carbon abundance at this time and is not a result of any gas-grain interactions. The abundance of the HCO^+ ion drops slightly at late times due to the depletion of its precursor molecule CO .

Examining the grain surface abundances of these species at late times, we see there is typically a much larger abundance present on the grain surface than in the gas phase. This is true for most of the neutral molecules, and is a result of desorption rates which are below the depletion rate, allowing the molecules to freeze onto the grain surfaces at early times when their abundances are peaking (e.g. C_2H , CO_2). Hence the grain surface holds these species as "fossil" remnants of early time chemistry. This is an example of the importance of the history of depletion process. This effect has been seen in other gas-grain networks (cf. Brown et al 1988a; Caselli et al 1993). The most abundant of the trace species in the carbon family present on the grain mantle is C_2H with a modest fractional abundance, $x(\text{C}_2\text{H}) \sim 2 \times 10^{-8}$ after 10^5 yr.

The lower panel of Figure 3 shows the time evolution of the chemistry for the same conditions at $\tau_V = 2.1$ msg. The gas phase evolution of these molecules shows the classic peak (following the neutral carbon abundance) and then the subsequent dramatic drop after $\sim 5 \times 10^5$ yr. Both gas phase and surface abundances exhibit the same time dependence as seen in the deeper regions of the cloud, with subsequently depressed abundances due to photodestruction.

The abundances of nitrogen bearing species are shown in Figure 4. Examining the top panel in Figure 4, at $\tau_V = 10.3$ msg. the nitrogen bearing species exhibit quite different temporal behavior depending on whether the molecule is linked to the carbon chemistry or not. The species which contain carbon, CN and HCN , show the same time dependent behavior as the CH compounds since these molecules can form via the interaction of nitrogen atoms with carbon radicals and ions. At later times, as the abundances of neutral carbon and carbon radicals sharply decrease, the abundances of HCN and CN rise

as the traditional equilibrium method for producing these molecules begins to dominate ($\text{HCNH}^+ + e^- \rightarrow \text{CN}, \text{HCN}$). In contrast, the nitrogen oxides and hydrides, NO , NH_3 , and N_2H^+ , show a steady rise in gas phase abundance. The significant increase of NH_3 abundance between 4×10^5 and 2×10^6 yr is due primarily to the formation of energetic N^+ ions from the destruction of N_2 by He^+ ions. The energetic N^+ ions have enhanced rates to react with hydrogen molecules which fuels the quick rise in the abundance of NH_3 (see Appendix A).

The evolution of the surface abundances for these species is highly dependent on the binding energy. The species with the highest binding energies, HCN and CN , show an abundance increase on the grain surfaces without reaching equilibrium. This is similar to the behavior exhibited by H_2O , the other strongly-bound species. For these species, the cosmic ray desorption timescale is greater than the depletion timescale, which results in an uninterrupted buildup on the mantle. The other neutral molecules, NO and NH_3 , have trace abundances on the mantle with $x(\text{NO})_{surf} \sim 10^{-7}$ and $x(\text{NH}_3)_{surf} \sim 10^{-8}$.

The time evolution at low visual extinction is presented in the bottom panel of Figure 4. In this figure, most of the nitrogen species are suppressed in both gas and surface phases, with most of the nitrogen residing in atomic form. This result is similar to that for oxygen where most of this species remains in atomic form because of strong photodestruction of O_2 coupled with cosmic ray desorption of O from the mantle. Since there is not sufficient molecular nitrogen present to form the energetic nitrogen ions required to produce NH_3 in the gas phase, the fractional abundance of NH_3 is quite low, $x(\text{NH}_3) < 10^{-11}$.

3.2. Optical Depth Dependence

In this section we discuss the effects of cloud optical depth upon our standard gas-

grain chemical model. The top panel in Figure 5 presents the profile distribution of abundances for the dominant species at $t = 10^5$ yr. Note that since we have not included a treatment of the photodissociation of H_2 , the abundances for species below $\tau_V < 0.5$ mag are overestimated. At this early time the molecules have not yet begun to deplete significantly, because the characteristic depletion time at this density is $\sim 10^6$ yr. Hence most of the species reside in the gas phase with only small abundances on the mantle. At 10^5 yr there are significant amounts of neutral carbon, oxygen, and nitrogen deep into the cloud. Significant differences can be observed at later times (lower panel) when many of the atoms have been converted to molecular form. As stated in the previous section, photodesorption, even with a yield as large as 10^{-4} is not as efficient as cosmic ray desorption in removing molecules from the mantle. For species such as CO and O_2 with moderate binding energies $E_b \sim 1000$ K (as opposed to H_2O , $E_b \sim 1800$ K), the cosmic ray desorption timescale is shorter than the photodesorption timescale for all cloud depths (at $n(\text{H}_2) = 10^4 \text{ cm}^{-3}$). Naturally, with higher yields or much larger radiation fields for photodesorption, this situation could change. However, photodesorption can be an important mechanism at the edge of clouds. Here, where photodesorption can play a role, molecular formation is strongly suppressed by photodestruction, decreasing the importance of photons removing molecules from the mantle.

Because of these effects the abundance profiles for both the gas phase and surface show distributions that exhibit a strong photochemistry. In general, the abundances of most species, except the self-shielding CO molecule, are suppressed at low τ_V and increase as the radiation field is attenuated. The grain surface abundances exhibit the same behavior as a function of extinction as the gas phase abundances. Therefore CO will dominate the grain surface until the radiation field is attenuated and allows molecules such as O_2 to form and deplete. For example, the abundance of both O_2 and N_2 in the gas phase are below 10^{-6} until $\tau_V \sim 2$ mag and then rise to their shielded values by τ_V

~ 6 mag.

The optical depth dependence for the less-abundant species is presented in Figures 6 and 7. One of the most interesting facets of this model, which can be seen in these figures, is that there are still appreciable abundances of many species in the gas phase. The grain surface abundances at 10^7 yr are slightly higher than those in the gas phase for most species since at $n(\text{H}_2) = 10^4 \text{ cm}^{-3}$ the depletion rate is larger than the desorption rate. *In spite of the inclusion of molecular depletion, abundances of observationally important species such as HCN, CN, NH₃, OH are in the range observed for cold shielded regions* (Irvine, Goldsmith & Hjalmarson 1987). However, the gas phase formaldehyde abundance in our model is too low by two orders of magnitude.

4. Discussion

We have presented gas phase chemical models including the effects of grain depletion and several desorption mechanisms. We have found that over a wide range of conditions cosmic ray spot heating is the most important desorption mechanism for $T_{dust} < 20$ K. The inclusion of cosmic ray desorption allows an active gas phase chemistry in spite of the high depletion rates at densities $> 10^4 \text{ cm}^{-3}$. To put these results into perspective, we will first compare our standard model results with chemical evolution without any grain processes. The work presented here is an attempt to model both gas phase and surface abundances therefore we compare our standard model to the pure gas phase ion-molecule results of Langer & Graedel (1989 [LG]) and the gas-grain chemical models of III. Second, we will discuss some of the observational consequences of our model, emphasizing in particular the effects of changing physical conditions and how these effects may be related to observations of molecular ice features in molecular clouds.

the gas phase chemistry to “overproduce” species at long times. The “overproduction” occurs due to the gas phase never reaching a true equilibrium because the grains act as sinks for any molecule produced by the gas phase ion-molecule chemistry which is still forming molecules at late times because the precursor atoms and ions are not depleted. It should also be noted that the metal ions show no evidence of depletion since their abundances do not differ drastically in comparing the models with grain accretion to those without grain accretion.

Comparison of our results with those of LG show some significant differences. First, our gas phase abundances of O_2 and H_2O with grains are still higher than those of LG. This is a consequence of our initial conditions in which we have much more oxygen available to react and form these species. However, in spite of these differences, there is nominal agreement for the nitrogen species, HCN , NO , and NH_3 . The glaring differences are that our model, with and without grain accretion, underproduces H_2CO , C_2H , HCO^+ , N_2H^+ , and CN in the gas phase when compared to LG. In addition the abundances of electrons and recombining ions are higher in our network than in LG.

Since metal ions are an important factor in deciding the ionization balance in molecular clouds (see Graedel et al 1982), the difference in abundance of metal ions between our results and the LG results is significant. Running our reaction network with all metals (S^+ , Fe^+ , Si^+ , Mg^+) depleted by an additional factor of ten changes the ionization balance and lowers the electron abundance from $x(e) = 1.4 \times 10^{-7}$ (standard model; at 10^7 yr) to $x(e) = 7.6 \times 10^{-8}$. The consequences of this change is to lower the dissociative recombination rates of polyatomic ions (e.g. H_3^+) which leads to a subsequent increase in their abundances. An illustration of the practical effects of depleting metals is shown in figure 6 where we show the HCO^+ abundance with metal ion abundances from table 1 and one run with metal ions depleted by a factor of ten (labeled “low metals”). In this figure the abundance of HCO^+ shows a dramatic increase (by about an order of

4.1. Comparison to Pure Gas Phase and Other Modeling Efforts

In Table 3 we list the abundances of selected species for our model run without gas-grain interactions as well as from our standard model with grain depletion and desorption. The abundances are listed at 10^7 yr since it is at this point when the gas phase evolution (without grains) reaches steady state. Also listed in the table are the results from LG and III. Since the models of LG and III are for well shielded regions, we present abundances at $\tau_V = 10.3$ mag. The physical conditions for LG and III are not exactly the same as our models with the main differences being the density, $5 \times 10^4 \text{ cm}^{-3}$ for LG, and $2 \times 10^4 \text{ cm}^{-3}$ for III, compared to our standard model of 10^4 cm^{-3} . LG also list their results at 108 yr but remark that their abundances are nearly constant after 107 yr. III use initial conditions similar to ours; however, we have a much larger oxygen pool than LG. In Table 3 we also list the abundances of the electrons and metal ions since these ions will be important for comparisons between networks.

The effects of grain depletion are easily seen in Table 3 when we compare the results for our model with and without grain depletion. The abundances of dominant molecular species such as CO, O₂ and N₂ show gas phase abundance reductions. However there are notable exceptions, for example, the abundances of most radicals are increased slightly or remain essentially constant (e.g. OH, NO, CN, and C₂H). These abundance enhancements occur in spite of the fact that total abundance of these species (gas + grain surface) is larger than that produced by the pure gas phase network without depletion. For example, the total abundance of CN both on grains and in the gas phase for the standard model is over an order of magnitude greater than that produced by the pure gas phase model. These effects are not limited to radicals: the abundance of H₂O on grains is two orders of magnitude greater than that produced without grain accretion. Hence one of the effects of including grains with cosmic ray desorption is to allow

magnitude) in the case where the metal abundances are lowered. Depleting the metals does reconcile some of our differences with LG for CN, HCO⁺ and N₂H⁺, but the H₂CO and C₂H abundances remain orders of magnitude below their result, reflecting actual differences between the two reaction networks.

The III model is slightly closer to our model because III include grain accretion and the same cosmic ray desorption rates. The main (and a significant) difference is that III have an extensive surface reaction network and thus it should not be surprising to find large differences between our results. In general, the abundances of most gas phase species in our models is larger than III, the main exceptions being NH₃ and CH₄. In our network cosmic ray desorption preferentially removes the weakly bound atoms from the grain surface allowing an active gas phase chemistry. In III, the atoms are rapidly processed into highly bound species on the surface via catalytic reactions. This results in H₂O being the dominant molecule on the grain surface in comparison to our standard model in which CO is most abundant species on the grain.

Another significant difference is that the III abundances of CO and O₂ in the grain mantles are orders of magnitude below our mantle abundances. For III, CO and O₂ are not abundant at long times because of slow hydrogenation with the main beneficiaries being H₂CO, CH₃OH, and H₂O (III; Herbst 1993). At 10⁶ years III has appreciable abundances of CO and O₂ in both the gas phase and on the grain surfaces. However, even at these early times our model predicts greater CO and O₂ abundances in both the gas phase and in the mantle.

The other important difference to note is the extremely low abundance of radicals for III since these species will quickly react on the grain surfaces. In our network the radicals are assumed to be inert on the grain surfaces.

4.2. Comparison to Gas Phase Observations in TMC-1

TMC-1 is a cold ($T_k \sim 10$ K), dense ($n(\text{H}_2) \sim 10^{11} \text{ cm}^{-3}$) condensation associated with Heiles Cloud #2. Since the physical conditions in TMC-1 are similar to our standard model for comparison we list in Table 3 the abundances of some species that have been observed in TMC-1. It should be noted that the observed abundances may only be accurate to within a factor of 10 (Irvine, Goldsmith, & Hjalmarsen 1987). With this in mind, we find agreement with observations for some of the simplest species CO, OH, CN, NO, NH_3 , and HCN. Our abundances are consistently below the observed values and the agreement is best for simple molecules whose chemistry is well known. We note that though we have presented these results at 107 yr the agreement with observations is qualitatively the same at 3×10^6 yr. Our model, at both 3×10^6 yr and 107 yr, predicts abundances of other species, such as H_2CO and C_2H , well below the observed limits. Additional changes in the initial conditions, such as a decrease in the abundance of metal ions by a factor of ten, would improve the agreement for some species. However, this study is not an attempt to accurately predict the abundances of all molecules observed in molecular clouds but rather an attempt to examine whether the gas phase chemical evolution can proceed with the inclusion of a realistic desorption model. We have presented our results at 107 yr to illustrate that the importance of the results is not the overall agreement or lack of agreement with the observations but that in spite of the high depletion rate at $n(\text{H}_2) = 10^{11} \text{ cm}^{-3}$, molecules are still present in the gas phase at late times and there is no dramatic disappearance of the gas phase as seen in Figure 1.

Some of the differences between our results and observations do merit further explanation. As we mentioned in the previous section our model does not predict enough H_2CO when compared to other chemical models. In fact both the models of both LG and Herbst & Leung (1989) predict an abundance of H_2CO close to the observed value in TMC-1. Thus we regard our low abundance of H_2CO a result of a deficiency in our

chemical reaction network and not a product of the gas-grain interaction. The situation for C_2H is quite different. The models of complex molecule formation of Leung, Herbst, & Huebner (1987) and Herbst & Leung (1989) find that the abundances of C_nH species best match observations with a time much earlier ($\sim 10^5$ yr) than presented in Table 3. In fact Herbst & Leung (1989) find that the best agreement for most species is at "early" times. These chemical studies are in agreement with the study of Olano, Walmsley & Wilson (1988) who estimated a lower limit to age of TMC-1 to be 2×10^5 yr. The study by Brown and Charnley (1989) who modeled the gas phase chemistry including depletion (with no desorption processes) also find better agreement with observations at early times prior to the onset of depletion. Our abundance predictions for some species would be in agreement at 10^5 yr. For example, the abundance C_2H at 10^5 yr is $\sim 8 \times 10^{-8}$. However the ages of molecular clouds are hard to categorize and the importance of our results is not the actual agreement at any particular time but that the chemical evolution actually continues at times significantly greater than the depletion timescale.

4.3. **Comparison of Our Model to Nonpolar and Polar Grain Components**

As mentioned in the introduction, observations of the absorption profile of CO ice suggests that surface CO is embedded into mantles of two distinct compositions. One component exhibits a weak, broad spectral feature (Sandford et al 1988); this is presumed to be CO embedded in a mantle dominated by polar molecules, presumably H_2O . The other spectral feature is a narrow, stronger component superimposed on the broad feature. The origin of this component is inferred to be CO ice in a matrix dominated by nonpolar species, which are possibly N_2 , O_2 , and CO_2 . These differences may be a result of differences of grain mantle composition along the line-of-sight (perhaps due to variations in the environment) and/or a consequence of abundance differences at the

time of mantle formation).

Our chemical model clearly applies to only the nonpolar component. For all relevant astronomical timescales, $t > 10^5$ yr, our static cloud model cannot reproduce mantles dominated by water ice, provided that the dust temperature in molecular clouds is < 20 K (see Table (i)). *Instead, our standard model for a high density region (shown in Figures 2-4) predicts that the grain mantles will be dominated by the highly abundant nonpolar species, CO and O₂ together with moderate amounts of H₂O and N₂.* At all times, the abundance of CO on the mantle is greater than that of H₂O and therefore in this model, the gas phase chemical evolution alone cannot reproduce observed H₂O abundances on grain mantles. Whittet (1993) finds an abundance of water frozen on grain surfaces from observations along lines of sight to field stars in Taurus to be $\sim 8.6 \times 10^{-5}$, which is significantly greater than our surface abundance at 10^7 yr of 1.1×10^{-5} .

This result lends credence to other studies which suggest most of the the observed H₂O ice on dust grains in molecular clouds is a result of reactions on the surface and not frosting from the gas phase (cf. Whittet 1993). Because we do not allow reactions on the mantle our model is somewhat inadequate to address this question. However, the models of I111 and IIII, which do allow reactions to proceed on the surface, cannot reproduce a mantle in which water *is not* the dominant constituent over CO.

Some gas-grain models which include surface reaction networks (Tielens & Hagen 1982; d'Hendecourt et al 1985) have been able to produce grain mantles where CO and O₂ are more abundant than H₂O. The required condition is a low rate of accretion for atomic H (Tielens et al 1991). In these models, if $n(\text{H}_2) > 10^4 \text{ cm}^{-3}$, then the abundance of atomic H is less than that of CO and O₂ in the gas phase. Hence the accreted CO and O₂ molecules will be more abundant than any other species on the mantle, provided most of the oxygen is contained in CO and O₂. Under these conditions, even if reactions occur on the mantle, most of the CO and O₂ will be inert on the mantle. Other less abundant

species may react on the mantle but since at these late times most of the carbon and oxygen is locked up in molecular form, it is unlikely that appreciable abundances of competing molecules such as H_2O will form. With these considerations in mind we will concentrate our discussion of surface abundance on only the dominant species on the mantle (CO , O_2 , H_2O). As such, our model is more representative of the nonpolar grains where H_2O is only a trace constituent, while Herbst (1993) has stated that the models of 1111 and 11111, apply to the polar component.

There is no direct evidence for molecules which comprise the nonpolar mantle because O_2 and N_2 are inactive in the infrared (d'Hendecourt et al 1985), while CO_2 features are obscured by the atmosphere. Currently the presence of these molecules must be inferred by examining subtleties in the CO absorption profile compared to profiles seen in the laboratory with different molecular mixtures. For example a mixture of solid $\text{O}_2:\text{CO}$ of 3:2 in the laboratory produces a spectra with a central wavelength $\lambda_0 = 4.678 \mu\text{m}$ and a FWHM $= 4.5 \text{ cm}^{-1}$ while the spectra of a mixture of $\text{CO}:\text{H}_2\text{O}$ 1:10 has $\lambda_0 = 4.672 \mu\text{m}$ and FWHM $= 4.5 \text{ cm}^{-1}$ (Tielens et al 1991; Kerr et al 1993). The changes in the laboratory spectra are often quite small and high resolution IR spectroscopy is required in order to differentiate them. Two high resolution spectroscopic studies of CO ice features have compared the observed absorption profiles with linear combinations of different laboratory spectra containing CO in several mixtures of O_2 , H_2O , and CO_2 . In Table 4 we present the results only for the mixtures which comprise the narrow nonpolar feature. It should be stressed that these comparison are limited by the number of laboratory studies that have been performed on possible interstellar ice mixtures (Kerr et al 1993).

Most of the sources in these studies are best fit with $\text{CO}:\text{H}_2\text{O}$ mantles with a ratio 10:1. Our standard model for $\tau_V = 10.3 \text{ mag}$ is consistent with these results yielding a ratio of $\text{CO}:\text{H}_2\text{O} = 10:0.2$ to $10:1.4$ between 10^6 and 10^7 yr . However we find a significant

amount of O_2 in the grain mantles for these times as well.

4.4. Comparison to Warm Star Forming Regions

In Section 4.2 we compared our gas-grain chemical model to observations from a dense cold dark cloud. However, in dense molecular core associated with newly-formed stars temperatures will be high enough to rapidly remove molecules from the grains and eject them in the gas phase. Examples of models of hot star forming regions are the studies of Brown, Charnley, & Millar (1988a,b) and Caselli et al (1993). Both of these studies examined the chemistry in the Orion hot core, including grain depletion and surface processes. These models follow the chemical evolution during the collapse of a cold clump of gas and dust where after a heating event associated with the formation of stars in the clump the grains are warmed significantly to release molecules into the gas phase.

our models are not as extensive as the previous examinations of Brown, Charnley, & Millar (1988) or Caselli et al (1993) since these studies included reactions on the grain surfaces and, in the case of Caselli et al (1993), had a more extensive reaction network. However it is worthwhile to examine the effects on the gas phase evolution by releasing molecules from the mantle. We have created a simple model by using the abundances of all species (gas and surface phases) at 10⁷ yr from the standard model of a quiescent cloud as initial conditions for another chemical model. Using these initial conditions we follow the time dependent chemical evolution and approximate the star “turn on” by instantaneously raising the dust temperature (at $t = 0$). Thus the picture is one of a quiescent cloud that at late times undergoes an instantaneous heating event caused by the formation of a star. The molecules will then be removed from the mantle at their respective thermal evaporation rate. This approximation is simplistic since a star will not simply “turn on” in this fashion nor do we consider the collapse of the cloud. It does, however, allow a first order examination of this complex situation).

To isolate effects of selective desorption we have chosen to examine $T_{dust} = 25$ K. For example, examination of Table 6 in Appendix B1 shows that a dust temperature of 25 K will desorb all of the CO and O₂ into the gas phase, while leaving HCN and H₂O on the mantle. Figure 8 shows the chemical evolution for selected species at $T_{dust} = 25$ K. In the upper panel see that by $t > 10^6$ yr all of the CO and O₂ have evaporated off the mantle while the abundance of H₂O on the mantle is constant and is actually rising on the grain mantle at late times. The gas phase abundances for these species shows the complementary picture with CO and O₂ increasing to their equilibrium values. However close examination reveals that by $\sim 10^6$ yr the abundance of O₂ is *decreasing*. This decrease in the abundance of this species is the result of chemical evolution that is not in equilibrium due to the presence of sinks for some species. The sinks are, of course, the grains which are selectively depleting the species which have large binding energies. Thus, the destruction of molecular oxygen in the gas phase, presumably by He ions, is fueling the growth of H₂O on the grain mantle. In fact, the abundance of H₂O in the gas phase at late times ($t > 10^6$ yr) is actually larger than that seen for the standard model at $T_{dust} = 10$ K.

A similar picture is seen in the lower panel, where molecules with intermediate binding energies slowly evaporate off the mantle (e.g. C₂H, CN) and the other species with higher binding energies (e.g. C₂O, HCN, and H₂CO) remaining on the mantle. The highly bound species, especially CO₂ show the same effects as seen for H₂O, gas phase abundance enhancements and growth on the mantle. The gas phase abundances of C₂H, HCN, CN, and NH₃ peak at $\sim 2 \times 10^5$ yr and then decrease. After this time the “normal” chemistry tries to reassert itself. For example, the “normal” quiescent evolution does not produce C₂H at late times because of the lack of atomic carbon. Since all of the atomic carbon is locked into CO when C₂H is desorbed from the grain mantles, it is rapidly destroyed via gas phase interactions.

Figure 9 shows another example of the star “turn on”, but modeled with $T_{dust} = 30K$. At this dust temperature most of the species are off the grain mantle by 10^6 yr and the chemistry is nearing a normal steady state solution. Thus, for not dust and $t > 10^6$ yr, the abundance enhancements from early time grain mantle evaporation (without surface processes) do not prevent the chemistry from proceeding to a normal pure gas phase steady state solution.

Since we have modeled only a quiescent cloud mildly heated by nearby stars, our results are difficult to compare quantitatively with observations. For example in the Orion hot core, where the best evidence exists for grain mantle evaporation, the temperatures are $T_k > 100$ K much higher than modeled in this work. In addition, the Orion hot core has large abundances of complex molecules that are not included in our reaction network. The star “turn on” model best represents warm regions that have been heated to temperatures < 50 K as the results of the formation of nearby stars. As such, we have chosen to compare our abundances with the extended quiescent ridge in Orion rather than the hot core. Mezger, Wink, & Zylka (1990) estimated a dust temperature of ~ 20 K for the extended Orion molecular cloud using the $350\mu m/1300\mu m$ ratio. Additional measurements of the gas temperature along the Orion ridge show that the temperature of the dense gas varies from 50 K near the Trapezium and the embedded BN/KL cluster, to 20 K further away from the heating sources (Bergin et al 1994). If $T_{dust} \approx T_{gas}$ along the dense ridge of gas, as is expected in these dense regions (Goldsmith and Langer 1978), then the Orion ridge may be an example of a region newly heated by forming stars.

Table 5 presents the abundances from the star “turn on” model along with abundances from the standard model at 10^7 yr and observed abundances from the Orion ridge. The agreement between observations and model is quite good. In fact, the model that includes grain mantle evaporation better matches observations than does the quiescent

gas model at $T_{dust} = 10$ K. However the number of species we compare is quite small and more detailed modeling including sulfur bearing species would be useful. In addition, we note that the early time ($\sim 10^5$ yr) models of Herbst and Leung (1989), who modeled the chemistry without any interactions with grains, are in just as good agreement with observations as are our results. As such, we regard the results from this crude model of heated gas as merely suggestive that the processes we have included may be ongoing in the warm dense regions of interstellar clouds as exemplified by the Orion ridge near the Trapezium stars.

4.5. The Dependence of Depletion on Physical Conditions and Its Relationship to Observations of Solid State Features

Depletion is highly dependent on the physical conditions of the parent cloud. Some details of this relationship have been presented in Appendix B, in which we examine the dependence of depletion on the dust temperature, radiation field, and the density. In this section we examine how our results apply to the observations of molecular ice features. In the following paragraphs we will refer to depletion as defined by the percentage of the total abundance of a species (gas phase + surface abundance) that is present on the grain surface. A molecule that shows a depletion of 90% will have 90% of the total abundance of that species on the grain surface and would be considered significantly depleted from the gas phase.

4.5.1. Density

Observations along lines of sight towards field stars in Taurus by Whittet et al (1989) have revealed depletions on the order of 5 - 40%. Since these results are towards obscured

stars that are presumably not associated with the cloud it is likely that they are probing quiescent material. Thus we might assume that a dust temperature of 10 K may be representative for the observations towards the most obscured stars which exhibit the highest depletions. With this assumption it is worthwhile to examine at what density our model agrees with the observed CO depletions, and whether at these densities millimeter observations may miss a significant fraction of molecular material.

To illustrate this, we plot in Figure 10 the depletion as a function of density to examine at what density different molecules will be significantly depleted from the gas phase. This figure shows that both CO and O₂ are quickly depleted below a level of 50% by $n(\text{H}_2) = 3000 \text{ cm}^{-3}$. While the highly bound species CN, HCN, and H₂O all show significant amounts of gas phase depletion for all densities. These results are uncertain since the depletion of a given species is a strong function of the binding energy and even a modest change in E_b (which are mostly unknown) will have a large effect.

Some binding energies have been measured in the laboratory for CO in an H₂O matrix (Sandford & Allamandola 1988) and CO in a pure CO matrix (Sandford & Allamandola 1988). We have used these binding energies to examine the interdependence of depletion and binding energy for the CO molecule. We present these results in Figure 11 showing depletion as function of density and binding energy. The dashed line in the figure is the nominal maximum depletion estimated by Whittet et al (1989) in Taurus. The most striking feature in this figure is that the CO molecule is easily accreted and held on a water mantle. In fact, for all densities, the depletions of CO in a water mantle are much larger than observed. Our model thus suggests that the CO ice observed in molecular clouds must be binding in a mantle with a binding energy much less than 1740 K. This conclusion is consistent with the observations of nonpolar and polar ice features, since CO is more abundant in the nonpolar layer which is not dominated by H₂O (Tielens et al 1991)

The binding of CO in the nonpolar mantle may also be inconsistent with the binding energies used in this work, which are for SiO₂ mantles. At high densities, even a binding energy for CO to an SiO₂ surface of ~ 1200 K produces high depletion. It is somewhat hard to categorize the actual densities along these lines of sight since space densities are difficult to infer from extinction measurements. However, various indications of the densities towards some of the field stars in Taurus are in the literature. Two of the stars in the survey by Whittet et al (1989), Elias 15 ($A_V = 13.3$ mag.) and Elias 16 ($A_V = 23.9$ mag.) are in portions of the Heiles' Cloud 2 mapped by Cernicharo, Guélin, & Askne (1984) in the $J = 1 - 0$ transition of HCO⁺ and its isotopic variant H¹³CO⁺. Both of these field stars are within the contours of the HCO⁺ emission (the beam size is $\sim 5'$) and Elias 15 is coincident with a local maximum in the H¹³CO⁺ map. These observations thus suggest the densities are $> 10^4 \text{ cm}^{-3}$ since HCO⁺ and in particular H¹³CO⁺ would be hard to excite at densities below this value. It is necessary to have more observations of high dipole moment molecules along these lines of sight where CO depletions are measured in order to better characterize the physical conditions.

If these densities are representative of the material where CO ice features are observed then pure CO ice seems to best reproduce observations. For CO-CO binding, depletions $> 50\%$ do not occur until $n(\text{H}_2) > 5 \times 10^4 \text{ cm}^{-3}$ which is not unrealistic for lines-of-sight with large extinction. In fact, for two sources listed in Table 4 the observations of the nonpolar component exhibit ice features consistent with pure CO ice. *If CO (or O₂) is the dominant component of the nonpolar ice then the binding energies for most species would be reduced to values that may allow a significant portion to remain in the gas phase, even at high densities.* Of Course these results are dependent on the desorption model and on the absence of competing reactions on the surface of the grain. However, given the current observations of CO ice features this question merits further exploration.

4.5.2. A_V Threshold

Both CO and H₂O ices exhibit a threshold value of visual extinction below which their ice features are not observed. In general this threshold is less for H₂O than for CO. In Taurus the water ice threshold is $A_V^{th} = 3.3$ mag while for CO, $A_V^{th} = 5.3$ mag (Whittet et al 1988, 1989). The extinction thresholds to observe CO and H₂O ices do vary from cloud to cloud (Williams, Hartquist, & Whittet 1992).

Several explanations for this effect have been proposed. Adamson et al (1988) propose that the thresholds suggest that the mantle desorption mechanism originates from the outside of the cloud. Williams, Hartquist, & Whittet (1992) attribute the desorption of H₂O to the local infrared radiation field. Duley and Williams (1993) proposed that the heat of formation of H₂O regulates this process for CO. While Smith, Sellgren, & Brooke (1993) suggest two separate mechanisms: for H₂O, photodesorption regulates mantle growth, while for CO simple thermal evaporation may be efficient.

Our single density cloud model shown in Figure 5 gives abundance profiles for both the gas and surface as a function of extinction. In this figure, due to self-shielding CO is abundant in the gas phase and on the grain surface at very low extinctions while H₂O does not appear in abundance on the mantle until $\tau_V = 4-5$ mag. These results seem contrary to observations where H₂O has a lower extinction threshold than CO. However we argued in Section 4.3 that our model cannot produce enough H₂O on the mantle to agree with observations. It is clear though, that a single density cloud model is not able to reproduce the observed extinction thresholds for CO.

Smith, Sellgren, and Brook (1993) noted that the dust temperature in Heiles' Cloud 2 as measured by the 60 μ m/100 μ m ratio is ~ 24 K (Snell, Heyer, & Schloerb 1989 [S11s]) at the cloud edges. Examining the dust temperature dependence in Table 6, $T_{dust} > 22K$ would be enough to desorb the volatile CO from the grain mantles. If

the dust temperature decreases with increasing extinction then a simple explanation for the CO threshold exists (i.e. dust temperature decreasing with distance into the cloud). There is evidence that the dust color temperature in Taurus and in other clouds, observed via the $60\mu\text{m}/100\mu\text{m}$ ratio, increases with *decreasing* column density (Heiles Cloud 2; S11S; B5; Langer et al 1989). In fact S11S show that the dust color temperature in Taurus is $> 20\text{ K}$ until $N(\text{H}_2) = 5 \times 10^{21} \text{ cm}^{-2}$, or $A_V = 5 \text{ mag}$. S11S and Langer et al (1989) also argue that only the smallest grains are responsible for the $60\mu\text{m}$ and $100\mu\text{m}$ emission. The larger grains, such as those responsible for molecular depletion, will be at lower temperatures and therefore will not have significant emission at $60\mu\text{m}$ and $100\mu\text{m}$. While the temperature of this component is uncertain it is likely that the larger grains will show the same temperature distribution with increasing column density as the smaller dust grains. Models of dust grains heated by the interstellar radiation field do show this dependence (de Muizon & Rouan, 1985). There is some evidence for the temperature of the colder dust component in the recent results from the longer wavelength survey of the galaxy at $140\mu\text{m}$ and $240\mu\text{m}$, by the Cosmic Background Explorer (COBE). This survey found that the average dust temperature in the molecular component of the inner galaxy is 19 K (Sodroski et al 1993). Since the dust emission is optically thin this dust temperature will reflect an average dust temperature over the presumably hotter cloud edges and the cooler interiors.

In our model CO is the dominant mantle constituent and as suggested in the previous sections the CO molecules will have a lower binding energy to a CO surface. In the case of pure CO ice the evaporation temperature is 17 K as opposed to $\sim 20\text{ K}$ for SiO_2 grains (see Table 6). Under these conditions the simplest solution for the CO extinction threshold is heating by the local radiation field as suggested by Smith, Sellgren, and Brooke (1993). The strong evidence that molecular clouds exhibit a clumpy structure (cf. Mundy et al 1986; Stutzki et al 1988; Stacey et al 1993) would only enhance these

effects. Variations in the threshold between clouds could then be related to changes in the fraction of material which resides in dense clumps.

5. Summary

We have presented here a model of gas phase chemistry for dense interstellar clouds including the effects of grain depletion and desorption. To assess the importance of different desorption mechanisms, we have included three potentially important mechanisms to remove species from the grain mantle: thermal evaporation, cosmic ray spot heating, and direct photodesorption. The chemistry has been examined using these desorption mechanisms in the context of a standard cloud model ($n(\text{H}_2) = 10^4 \text{ cm}^{-3}$, $T_{dust} = 10 \text{ K}$, $T_{gas} = 20 \text{ K}$, $\chi = 1.0$). These models of gas-grain chemical evolution are both time dependent and depth (τ_V) dependent. Using the standard model as a reference case, we have also examined the interdependence of the gas-grain interaction over a wide range of conditions by varying the density, dust temperature, and UV field enhancement. To isolate effects of gas phase and gas-grain interactions we exclude surface catalysis. We list the principal results below.

1) Over a wide range of conditions, $n(\text{H}_2) = 10^3 \text{ cm}^{-3}$ to 10^5 cm^{-3} , $T_{dust} < 20 \text{ K}$, and $\tau_V > 2 \text{ mag}$, we find that cosmic ray desorption is the most important mechanism for removing species from the grain surfaces.

2) Due to cosmic ray desorption, which functions even at large visual extinctions, at times greater than the depletion timescale at $n(\text{H}_2) = 10^4 \text{ cm}^{-3}$, an active gas phase chemistry persists, as shown in Figure 2. This is different from previous studies where the gas phase shows a dramatic disappearance. At these late times, the abundances of some simple species in the gas phase from the standard model are close to agreement with observations of abundances in TMC-1. The agreement is best for simple molecules

whose chemistry is fairly well known.

3) Examination of the dependence of depletion with density shows that several observationally important species, such as HCO^+ and HCN , exhibit gas phase abundance reductions when the density is increased from $n(\text{H}_2) = 10^3 \text{ cm}^{-3}$ to 10^5 cm^{-3} . Since depletion is strongly influenced by density a comparison of gas phase abundances between high densities and low densities may provide evidence of its effects.

4) For astrophysically relevant timescales ($t > 10^5 \text{ yr}$) we find that CO , and at $t > 10^6 \text{ yr}$, O_2 are the most abundant species on the grain mantles with trace amounts of H_2O and N_2 . We also find that depletion from the gas phase cannot reproduce the observed abundance of H_2O molecules on grain surfaces.

5) observations of CO ice features show that CO is embedded in two components: one dominated by non-polar species and the other by polar molecules, presumably H_2O . In the model presented here CO and the non-polar O_2 molecule are the dominant species on the mantle, thus our model applies to the non-polar grain component. Most of the observational studies of non-polar CO ice are best fit with $\text{CO}:\text{H}_2\text{O}$ mantles with a ratio of 10:1. Our results are in agreement with the observations. However we also find large amounts of O_2 present in the mantle.

6) We have examined the interdependence of CO depletion with gas density and binding energy and find that the observed depletion limit for CO in Taurus of 40 percent is inconsistent with CO bonding in an H_2O rich mantle. This result is in agreement with observations of solid CO , which suggest that most of the CO is in a mantle with only trace amounts of H_2O (Tielens et al 1991).

7) The results for CO binding to different grain surfaces show that depletion is highly dependent on the surface binding energy of the species, which are highly uncertain and depend upon which species is the dominant component of the grain mantle. In

almost every case presented here CO is the dominant species on the mantle. If the interstellar grain mantles consist of a layer of CO ice, then the binding energies for physical adsorption would be reduced to values that could allow a significant amount of this species to remain in the gas phase.

We would like to acknowledge Yves Viala and Jean Jacques Benayoun for providing the chemical network used in this work. We thank Gary Maroon for providing a key portion of the code. We are also indebted to Al Glassgold for providing information on the activation barriers on neutral-neutral reactions. F. A. B. is grateful to Doug Whittet for a very useful discussion of observations of molecular ice features. We would like to thank Mark Allen, especially for his comments on the binding energies, and Ron Snell for numerous useful discussions on observations and chemistry in molecular clouds. The research at the University of Massachusetts was supported by a grant from the National Aeronautics and Space Administration (NASA) for the Submillimeter Wave Astronomical Satellite. This work was conducted in part at the Jet Propulsion Laboratory, California Institute of Technology under contract to the NASA. The National Astronomy and Ionosphere Center is operated by Cornell University under a cooperative agreement with the National Science Foundation.

Appendix A

Changes To THE Viala Database

We have made several changes and additions to the database compiled by Viala (1986) and Benayoun et al (1991) which we list below.

1) The network has been revised to include the enhanced reaction rates at low temperatures between ions and high dipole moment neutral molecules using the formalism of Millar et al (1991).

2) Considerable attention has been focused on the reactions which initiate the chemistry of nitrogen hydrides. Unlike reactions that initiate the carbon and oxygen chemistry, the reaction of N with H_3^+ possesses a large activation barrier (Herbst, DeFrees, and McLean 1987) and therefore cannot be a major formation pathway in the low temperature environments of molecular clouds. Rather, the formation of nitrogen hydrides is believed to be initiated by the reaction $\text{N}^+ + \text{H}_2 \rightarrow \text{NH}^+ + \text{H}$ (Herbst, DeFrees, and McLean 1987; Galloway and Herbst 1989, Le Bourlot 1991). This reaction has been studied at low temperatures in the laboratory and has been found to be slightly endothermic with an activation barrier of ~ 210 K (Luine and Dunn 1985; Marquette et al 1985; Marquette, Rebrion, and Rowe 1988). This presents a complication for forming NH_3 since under normal quiescent interstellar conditions ($T_k \sim 10$ K) this small activation barrier would suppress the reaction sequence that ultimately forms ammonia.

Many theoretical and experimental efforts have been directed to studying this important reaction (Luine & Dunn 1985; Ervin & Armentrout 1987; Yee, Lepp, & Dalgarno 1987; Galloway and Herbst 1989). Adams, Smith, & Millar (1984) have suggested that if the N^+ ions are formed via dissociative ionization by He^+ of nitrogen molecules (N_2 , CN , etc.), rather than by cosmic ray ionization of N, then the product N^+ ions may have

enough translational energy to overcome the activation barrier and allow this reaction to proceed.

The theoretical calculations of Galloway & Herbst (1989, [GII]), provide an avenue for facile intrusion of these complications into a chemical network. They present theoretical rate coefficients for the $N^+ + H_2$ reaction under both thermal and non-thermal conditions. Under thermal interstellar conditions ($T_k = 10 - 20$ K), the N^+ ions are created mainly by cosmic ray ionization and the reaction rate is small ($k < 10^{-13}$ cm³s⁻¹) in agreement with previous results by Herbst, DeFrees, & McLean (1987). Under non-thermal conditions, the N^+ ions are the product of dissociative ionization and are imparted with non-thermal translational energy that may overcome the barrier. The reaction rate under these conditions depends upon the spin orbit energy distribution of the energetic N^+ ions and is a fraction of the Langevin rate ($k_{Langevin} = 1.6 \times 10^{-9}$ cm³s⁻¹).

Rather than treating the abundances of the thermal and non-thermal N^+ ions as separate species we have opted to use the thermal rate (see Table 3 of GII) at early times when N^+ is formed mainly via cosmic ray ionization. When the production rate of the N^+ by dissociative ionization of N_2 , NO, HCN, and CN exceeds the formation rate by cosmic rays we have used the larger rates for non-thermal N^+ from Table 4 of GII, assuming an LTE energy distribution of the N^+ spin states. Hence, when the following inequality is satisfied in the time dependent computation of abundances the higher non-thermal rates are used:

$$([N_2] + [NO] + [HCN] + [CN])[He^+]k_{diss} \geq \zeta_N [N]$$

where the brackets denote space density of a given species, k_{diss} is a characteristic dissociative ionization rate ($k_{diss} = 3.0 \times 10^{-9}$ cm³s⁻¹), and $\zeta_N = 2.72 \times 10^{-17}$ s⁻¹ is the

cosmic ray ionization rate of nitrogen. The practical effect of this approximation is a longer formation timescale for ammonia compared to other simple nitrogen molecules such as NO or CN.

3) We have removed the neutral-neutral reactions $C_2 + H_2 \rightarrow C_2H + H$ and $C_2H + H_2 \rightarrow C_2H_2 + H$ from the Viala network because of concerns about the likelihood of activation barriers. An activation barrier of ~ 1400 K has been estimated for the latter reaction by Brown & Laufer (1981).

4) Low temperature measurements of the reaction of $C_2H_2^+$ with H_2 show an enhanced rate. Therefore we have included this reaction which produces $C_2H_3^+$ and H with a rate of $5.6 \times 10^{-11} T_k^{-2} \text{ cm}^3 \text{ s}^{-1}$ (Hawley & Smith 1992; Glassgold, Omont, & Guélin 1992).

5) A large amount of attention has been focused, in both laboratory measurements and theoretical calculations, on the dissociative recombination rate for H_3^+ . This ion is quite important since it initiates the formation of carbon and oxygen bearing molecules (Graedel, Langer, & Frerking 1982). The rate for this reaction has undergone numerous revisions in the past decade (cf. Adams & Smith 1988; Canosa et al 1991). We have adopted a rate of $1.5 \times 10^{-7} (T_k/300)^{0.5} \text{ cm}^3 \text{ s}^{-1}$ based on the measurements of Canosa et al (1991).

6) Of considerable importance in the model is the inclusion of the CO self-shielding. Since carbon monoxide is the only molecule observed in regions of low extinction in both the gas and the solid phase (Whittet et al 1989) it is quite important to treat correctly CO photodestruction. We have used rates for CO photodissociation presented in van Dishoeck & Black (1988) which include an approximation to the effects of self-shielding. In this parameterization the photodissociation rate separately accounts for the effects of dust continuum absorption, which is dependent on the visual extinction, and that of self shielding, which is dependent on the total CO and H_2 column densities.

Appendix B

PARAMETER VARIATIONS

In this Appendix we examine the effects of varying T_{dust} , χ , and β (112). For the most part we will restrict our discussion only to those species which are the dominant reservoirs of carbon, oxygen, and nitrogen.

131. DUST TEMPERATURE

Dust temperatures inside molecular clouds typically vary between 5 - 30 K depending on the proximity of heating sources. This variation can influence the desorption of molecules by changing the rate of thermal evaporation. The rate for thermal evaporation, which is negligible at $T_{dust} = 10$ K, is proportional to $\exp(-E_b/T_{dust})$, hence warming up grains by even a modest amount can have a significant effect on removal of molecules from the mantle. We have modeled the gas-grain chemical evolution over a range of dust temperature in order to examine the dependence of surface and gas composition on T_{dust} .

The top panel in Figure 12 shows the abundance profile at $T_{dust} = 20$ K and 107 yr for the major reservoirs of carbon, oxygen, and nitrogen. Raising the dust temperature from 10 K (shown in Figure 5) to 20 K does not have a major effect upon the chemistry. For example, the abundance of CO in the gas phase is increased by a factor of two with the difference coming solely from CO molecules evaporating off the grain surface. A similar change in abundance is seen for molecular oxygen and nitrogen. In contrast, the strongly-bound species show only small gas phase enhancements; for H₂O the gas phase abundance increases by only a factor of 1.5.

The behavior changes dramatically when T_{dust} is increased above ≈ 22 K. At 30 K (shown in the lower panel) the surface composition is greatly modified with only H₂O

remaining on the mantle. To examine the surface composition more closely we list in Table 6 the percentage of the total abundance of a several species which is in the gas phase for several values of the dust temperature. The percentage in the gas phase is defined as $100 \times (\text{gas phase abundance}) / (\text{gas phase abundance} + \text{surface abundance})$. The second column in Table 6 shows the percentage in the gas phase for $T_{dust} = 0$ K; these values represent the results solely of desorption by cosmic rays without any contribution by thermal evaporation or photodesorption (which is not significant at $\tau_V = 10.3$). The percentages listed in Table 6 show that gas phase depletion is highly sensitive to the dust temperature. The amount of CO and O₂ in the gas phase is quite stable and large until $T_{dust} > 18$ K, above this temperature the amount in the gas phase shows a significant increase so that by $T_{dust} = 22$ K virtually all of the CO and O₂ are removed from the grain surface. Depletion is also acutely affected by the chosen binding energies. The species in the table are listed in order of increasing binding energy and show that at a dust temperature < 30 K some species will be selectively depleted from the gas phase solely because of strong binding to the grain surfaces. For example, for dust temperatures as high as 30 K, the abundance of water in the gas phase is strongly depressed and the grains will act as a sink for any H₂O molecules created, but molecules with $E_b < 1500$ K will reside essentially only in the gas phase.

132. DENSITY

Chemical abundances and evolutionary timescales are sensitive to density due to increased collision rates in the gas and on the grain surfaces. In Table 7 we list gas and grain abundances for a number of species. We have chosen to present these results at 10^6 yr since this will show the effects of the changing depletion timescale, which is greater than 10^6 yrs for $n(\text{H}_2) = 10^5 \text{ cm}^{-3}$ and $< 10^6$ yrs for $n(\text{H}_2) = 10^4 \text{ cm}^{-3}$. In Table 7 the abundances of the major reservoirs show, as expected, greater depletion on

grains for higher densities. For example, the surface abundance of CO and O₂ show a steady decrease in gas phase abundance, coupled with consistent build up of mantle abundances. However, many of the trace reactive species, such as C₂H, show significant decrease in gas phase abundance between densities of 10³ and 10⁷ cm⁻³ both due both to destruction by gas phase reactions and to depletion on grains. The abundances of HCO⁺ and N₂H⁺ are also sharply decrease over several orders of magnitude for higher densities. This decrease is due to a combination of the reduction in the abundance of H₃⁺, which is inversely dependent on density, and to gas phase depletion of the precursor molecules CO and N₂.

B3. RADIATION FIELD

In section 3 we presented cloud models using only the normal interstellar radiation field. As such these models are more representative of dark clouds which are not associated with nearby bright stars or embedded young stellar objects. Since there are numerous dense cores associated with luminous young stars that enhance the local radiation field we have examined the dependence of the chemistry with enhanced ultraviolet flux. Figure 13 show the abundance profiles for selected species at 10⁷ yr with an enhancement factor of $\chi = 100$. As seen in the standard model with $\chi = 1$ the behavior of abundance with depth is influenced strongly by the photodissociation of molecules. With $\chi = 100$ the transition region in Figure 13a from atomic to molecular form shifts $10 \tau_V \sim 5$ mag from $\tau_V \sim 6.5$ mag for the oxygen and nitrogen molecules. Because of enhanced photodissociation rates the abundances of most neutral species on grain mantles are much lower until the radiation field is significantly attenuated deeper in the cloud.

It is worthwhile to note that species that are linked to the carbon chemistry via C⁺ (e.g. CO, CN, and C₂H) show large abundance in the gas phase at very low extinctions $\tau_V < 2$ in spite of the high photodestruction rates. CO is formed with a large abundance

at $\tau_V = 1.5$ mag via the sequence $C^+ + OH \rightarrow HCO^+$ followed by dissociative recombination. While the sequences that form CN and C_2H start with the same initial reaction: $C^+ + CH_2 \rightarrow C_2H^+ + C$, C_2H^+ is destroyed in two ways which eventually results in the formation of C_2H and CN. As the abundance of C^+ drops with increasing extinction, the abundances of CO, CN, and C_2H decrease as the above rates diminish and their production makes a transition switch to other pathways relevant at high extinction.

The abundances of CO, CN, and C_2H on the grain mantles are also slightly reduced due to photodesorption. This is due to the increased rate of photodesorption, which for $\chi = 100$ is greater than the rate of desorption by cosmic rays for $\tau_V < 2.6$ mag. Thus photodesorption is important for species which are abundant at low extinction because of formation paths linked to C^+ . In Figure 13 the abundances of CO, CN, and C_2H are larger in the gas phase than on the surface. Other molecules such as O_2 and H_2O will not form until $\tau_V > 4$ because of increased photodestruction rates.

This illustrates the importance of the photodesorption yield, the value of which (as stated in section 2.2.2) is highly uncertain. In our calculations (with a yield of 10^{-4}) photodesorption is an efficient desorption mechanism only for low extinctions and very high radiation fields and only for a select group of molecules. However a larger yield of $\sim 10^{-2}$, as suggested by Greenberg (1973), combined with an enhanced radiation field, would lead to a desorption rate that is higher than the depletion rate up to $\tau_V \sim 4.3$ mag without any change in photodestruction rates. Photodesorption may thus begin to inhibit mantle formation at these depths for even the easily-depleted H_2O molecule.

Table 1

Initial Elemental Abundances and Depletion Factors ^a

Element	δ_X^b	Abundance (Relative to H ₂)
C ⁺	2(-1)	1.0(-4)
N	2(-1)	4.5(-5)
O	2(-1)	3.5(-4)
S ⁺	1 (-2)	1 .6(-7)
Si ⁺	2(-4)	1 .6(-8)
Mg ⁺	4(-3)	3.0(-7)
Fe ⁺	3(-3)	2.0(-7)

^aNumbers are written in the form a(-b) = a x 10^{-b}.

^bDepletion Factor defined as $\delta_X = I_i(X)/I_i(X)_O$

Table 2

Relevant Timescales in yrs. ^a			
Timescale	C	CO	H ₂ O
τ_{dep}^b	7.8(5)	8.6(5)	6.9(5)
$\tau_{ph}(A_v = 2.0)$	6.0(7)	6.0(7)	6.0(7)
τ_{cr}^b	7.4(3)	2.2(6)	1.3(10)

^aNumbers are written in the form a(b) = a x 10^b

^b τ_{dep} and τ_{cr} calculated at $11(112) = 10^4 \text{ cm}^{-3}$

Table 3
Comparison of standard model with pure gas phase and other chemical models
Fractional Abundances at 10^7 yrs. ^a

Species	without grains	with grains		I.G (Run 6)	III Model N(2100,CR)		TMC - 1 ^b
	Gas	Gas	Surface	Gas	Gas	Surface	Gas
C	3.7(-10) ^c	1.4(-9)	1.8(-11)	3(-8)	6.6(-10)	3.5(-11)	
C ⁺	6.5(-10)	1.0(-9)		3(-9)	3.1(-12)		
CO	1.0(-4)	2.8(-5)	7.1(-5)	7(-5)	1.1(-9)	4.8(-10)	8(-5)
O ₂	9.5(-5)	2.8(-5)	7.2(-5)	6(-6)	1.0(-11)	1.6(-12)	
H ₂ O	9.4(-7)	4.0(-7)	1.0(-5)	9(-8)	2.1(-9)	2.0(-4)	
OH	3.9(-8)	4.9(-8)	2.4(-7)	7(-9)	1.6(-9)	2.9(-20)	3(-7)
O	5.8(-5)	3.8(-5)	5.0(-7)	2(-5)	7.5(-10)	4.2(-23)	
N ₂	1.0(-5)	4.2(-6)	1.0(-5)	6(-6)	9.4(-7)	1.1(-6)	
N	2.3(-5)	1.4(-5)	1.9(-7)	3(-5)	3.4(-7)	7.1(-16)	
C ₂ H	7.3(-12)	2.4(-11)	2.3(-8)	2(-9)	1.7(-12)	7.6(-24)	8(-8)
C ₂ H ₂	2.2(-12)	9.7(-12)	2.9(-9)		2.4(-11)	3.6(-11)	
C ₂ H ₄	5.0(-14)	5.8(-14)	2.2(-12)		3.7(-8)	3.8(-6)	
CO ₂	7.3(-10)	5.1(-11)	6.6(-9)		9.2(-15)	2.1(-5)	
H ₂ CO	8.9(-12)	3.6(-12)	1.5(-10)	1(-9)	2.7(-11)	4.2(-5)	2(-8)
HCO ⁺	9.3(-10)	4.7(-10)		4(-9)	8.3(-13)		8(-9)
NO	6.1(-8)	7.2(-8)	1.8(-7)	7(-8)	4.3(-11)	6.6(-14)	< 3(-8)
NH ₃	3.2(-8)	2.3(-8)	1.4(-8)	6(-9)	9.2(-7)	2.8(-6)	2(-8)
CN	2.1(-9)	4.0(-9)	5.7(-8)	8(-8)	2.9(-10)	7.1(-22)	3(-8)
HCN	1.7(-9)	1.9(-9)	3.4(-8)	1(-9)	1.8(-10)	5.9(-6)	2(-8)
N ₂ H ⁺	3.9(-11)	2.9(-11)		1(-10)	3.1(-10)		5(-10)
He ⁺	4.4(-10)	8.2(-10)		3(-10)	3.8(-9)		
H ₃ ⁺	2.4(-9)	3.9(-9)		3(-9)	5.6(-8)		
e	3.4(-7)	3.2(-7)		6(-8)	4.6(-8)		
S ⁺	3.5(-8)	5.0(-8)		3(-10)	1.4(-15)		
Si ⁺	8.4(-9)	8.1(-9)		7(-9)	5.9(-20)		
Mg ⁺	1.5(-7)	1.1(-7)		4(-8) ^c	9.9(-12)		
Fe ⁺	1.4(-7)	1.4(-7)			1.9(-9)		

^aNumbers are written in the form a(-b) = a × 10^{-b}.

^b TMC - 1 abundances from Irvine, Goldsmith, & Hjalmarsen (1987) except NO (McGonagle et al 1990).

^c This number represents the sum of the abundances of heavy metal ions including Mg⁺ and Fe⁺.

Table 4

Summary of Observations of <u>Nonpolar CO Component</u> <u>011 Grains</u>					
ρ Oph	Elias 29	CO:H ₂ O	(10:1)	embedded	Kerr et al (1993)
	Elias 32	Pure CO		embedded	
	VS 17	CO:H ₂ O	(10:1)	embedded	
	WL 5	CO:H ₂ O	(10:1)	embedded	
	WL 6	CO:H ₂ O	(10:1)	embedded	
	WL 12	CO:H ₂ O	(10:1)	embedded	
Serpens	CK 2	Pure CO		field	Chiar et al (1994)
	CK 3	CO:H ₂ O	(10:1)	embedded	
	SVS4 S	CO:O ₂	(3:2)	embedded	
.. — — —	SVS4 N	CO:O ₂	(3:2)	embedded	— — —

Table 5
 Fractional Abundances at 10^5 yr with Star Turn On^a

Species	^b $T_{dust} = 10$ K	$T_{dust} = 25$ K	$T_{dust} = 30$ K	^c Orion Ridge
CO	2.8(-5)	1.0(-4)	1.0(-4)	8(-5)
C ₂ H	7.3(-12)	3.2(-8)	2.8(-8)	1.0(-8)
HCO ⁺	4.7(-10)	1.4(-9)	1.4(-9)	3.0(-9)
NO	7.2(-8)	2.0(-7)	2.2(-7)	<5.0(-8)
NH ₃	2.3(-8)	1.2(-7)	1.2(-7)	2.0(-7)
CN	4.0(-9)	2.9(-8)	4.7(-8)	5.0(-9)
H ₂ CN	1.9(-9)	8.6(-9)	1.6(-8)	2.0(-8)
N ₂ H ⁺	2.9(-11)	1.0(-10)	1.0(-10)	2.0(-10)

^aNumbers are written in the form $a(-b) = a \times 10^{-b}$.

^bfrom standard model at 10^7 yr

^cOrion abundances from Blake et al (1987)

Table 6
 Percentage in the gas phase for various species as a function of T_{dust}
 at 10^7 yrs with $n(\text{H}_2) = 10^4 \text{ cm}^{-3}$, $T_{gas} = 20 \text{ K}$, $\chi = 1.0$

$T_{dust} =$ Species	0 K	16 K	18 K	20 K	22 K	24 K	26 K	28 K	30 K	$E_{bind}(K)$	
NH ₃	61	61	64	99	100	100	100	100	100	1082	
CO	28	28	28	50	99	100	100	100	100	1181	
O ₂	28	28	28	50	99	100	100	100	100	1181	
C ₂ H	<	1	<1	<1	<1	<1	18	81	100	100	1427
CN	7	7	7	7	6	10	87	100	100	1476	
HCN	5	5	5	5	6	6	6	10	79	1722	
H ₂ CO	2	2	2	3	4	4	4	7	79	1722	
H ₂ O	4	4	4	4	5	5	5	5	13	1820	

Table 7
 Fractional Abundances at 10⁷ yr and $T_{dust} = 10$ K^a

Species	$n(H_2) = 1 \times 10^3 \text{ cm}^{-3}$		$n(H_2) = 3 \times 10^3 \text{ cm}^{-3}$		$n(H_2) = 1 \times 10^4 \text{ cm}^{-3}$		$n(H_2) = 1 \times 10^5 \text{ cm}^{-3}$	
	Gas	Surface	Gas	Surface	Gas	Surface	Gas	Sil'fac'
C	1.1(-6)	1.5(-9)	8.3(-9)	3.6(-11)	4.8(-10)	6.4(-12)	5.6(-11)	2.3(-12)
CO	9.1(-5)	7.7(-6)	7.7(-5)	2.3(-5)	4.3(-5)	5.7(-5)	3.8(-5)	9.6(-5)
CH	1.2(-9)	1.8(-13)	9.4(-11)	4.2(-14)	1.8(-11)	2.8(-14)	5.6(-12)	8.3(-14)
O ₂	2.3(-5)	1.1(-6)	2.8(-5)	3.1(-6)	3.5(-5)	1.4(-5)	8.9(-6)	9.3(-5)
H ₂ O	1.0(-6)	1.5(-7)	1.0(-6)	3.5(-7)	1.2(-6)	1.3(-6)	2.6(-7)	1.2(-5)
C ₂ H	9.1(-10)	8.7(-9)	3.7(-11)	1.4(-8)	2.0(-11)	2.7(-8)	3.8(-11)	2.21(-7)
C ₂ H ₂	5.5(-10)	1.4(-9)	1.4(-11)	1.9(-9)	2.1(-12)	2.9(-9)	1.1(-11)	1.1(-8)
H ₂ CO	2.3(-11)	2.5(-11)	6.0(-12)	4.1(-11)	4.6(-12)	1.0(-10)	7.0(-13)	8.8(-10)
HCO ⁺	3.7(-9)		1.5(-9)		5.5(-10)		6.1(-11)	
N ₂ H ⁺	1.1(-11)		1.1(-11)		9.0(-12)		7.7(-12)	
NH ₃	4.2(-9)	1.9(-10)	3.9(-9)	3.9(-10)	4.5(-9)	1.5(-9)	2.8(-9)	1.0(-8)
CN	9.7(-9)	1.1(-8)	8.8(-10)	1.1(-8)	1.6(-10)	1.1(-8)	6.6(-11)	1.1(-8)
HCN	3.6(-9)	2.6(-9)	8.6(-10)	4.6(-9)	3.6(-10)	1.0(-8)	1.1(-10)	7.0(-8)
OH	1.5(-7)	1.9(-8)	6.4(-8)	2.3(-8)	2.9(-8)	3.1(-8)	1.1(-8)	9.6(-8)

^aNumbers are written in the form a(-b) = a x 10^{-b}.

References

- Adams, N. G., Smith, D., & Millar, T. J. 1984, MNRAS, 211, 857
- Adams, N. G., & Smith, D. 1988, in *Rate Coefficients in Astrochemistry*, eds. T. J. Millar & D. A. Williams (Dordrecht: Kluwer).
- Adamson, A. J., Whittet, D. C. B., Bode, M. F., Longmore, A. J., Roche, P. F., McFadzean, A. D., Geballe, T. R., & Aitken, D. K. 1988, in *Dust in the Universe*, eds. M. E. Bailey & D. A. Williams, (Cambridge: Cambridge University Press), 61.
- Allen, M., & Robinson, G. W. 1977, ApJ, 212, 396.
- Bates, D. R., 1991, J. Phys. 1], 24, 3267,
- Benayoun, J. J., Nercessian, E., & Violla, Y. P. 1991, *Chimie interstellaire et circumstellaire*, Technical memorandum, University of Grenoble.
- Blake, G. A., Sutton, E. C., Masson, C. R., Phillips, T. G. 1987, ApJ, 315, 621
- Bourdon, E. B., Prince, R. H., & Duley, W. W. 1982, ApJ, 260, 909.
- Brown, R. L., & Laufer, A. H. 1981, J. Phys. Chem., 85, 3826.
- Brown, P. D., Charnley, S. B., & Millar, T. J. 1988a, in *Rate Coefficients in Astrochemistry*, eds. T. J. Millar & D. A. Williams, (Dordrecht: Kluwer), 263.
- Brown, P. D., Charnley, S. B., & Millar, T. J. 1988b, MNRAS, 231, 409.
- Brown, P. D., & Charnley, S. B. 1990, MNRAS, 244, 432.
- Canosa, A., Rowe, B. R., Mitchell, J. B. A., Gomet, J. C., & Rebrion, C. 1991, A&A, 248, L19.
- Caselli, P., Hasegawa, T. I., & Herbst, E. 1993, ApJ, 408, 548.

- Cernicharo, J., Guélin, M., & Askne, J. 1984, *A&A*, 138, 371.
- Charnley, S. B., Dyson, J. E., Hartquist, T. W., & Williams, D. A. 1988, *MNRAS*, 231, 269.
- Chiar, J. E., Adamson, A. J., Kerr, T. H., & Whittet, D. C. B. 1994, in press.
- de Muizon, M., & Rouan, D. 1985, *A&A*, 143, 160.
- Draine, B. T., & Salpeter, E. E. 1979, 231, 438.
- Duley, W. W., & Williams, D. A. 1993, *MNRAS*, 260, 37.
- Ervin, K. M., & Armentrout, T. B. 1987, *J. Chem. Phys.*, 86, 2659.
- d'Hendecourt, L. B., Allamandola, L. J., & Greenberg, J. M. 1985, *A&A*, 152, 130.
- Galloway, E. T., & Herbst, E. 1989, *A&A*, 211, 413.
- Gear, C. W. 1971, *Numerical Initial Value Problems in Ordinary Differential Equations*, (Englewood Cliffs, N. J.: Prentice-Hall).
- Glassgold, A. E., Omont, A., & Guélin, M. 1992, 396, 115.
- Graedel, D. E., Langer, W. D., & Freking, M. A. 1982, *ApJS*, 48, 321.
- Greenberg, J. M. 1973, in *Interstellar Dust and Related Topics*, IAU Symp. No. 52, eds. J. M. Greenberg & H. C. van de Hulst, (Dordrecht: Reidel), 431.
- Habing, H. J. 1968, *Bull. Astr. Inst. Netherlands*, 19, 421.
- Hartquist, T. W., & Williams, D. A. 1991, *MNRAS*, 247, 343.
- Hasegawa, T. I., Herbst, E., & Leung, C. M. 1992, *ApJS*, 82, 167.
- Hasegawa, T. I., & Herbst, E. 1993, *MNRAS*, 261, 83.

- Hawley, hi., & Smith, M. A. 1992, *J. Chem. Phys.*, 96, 1121
- Herbst, E., DeGreys D. J., & McLean, A. D. 1987, *ApJ*, 321, 898.
- Herbst, E. & Leung, C. M. 1989, *ApJS*, 69, 271.
- Herbst, E. 1993, in *Dust and Chemistry in Astronomy*, eds. 'T. J. Millar & D. A. Williams, (Institute of Physics Publishing: Bristol), 183.
- Hindmarsh, A. C. 1980, *ACM SIGNUM Newsletter*, 15, 10.
- Hollenbach, D., & Salpeter, E. E. 1970, *J. Chem. Phys.*, 53, 79.
- Iglesias, E. 1977, *ApJ*, 218, 697.
- Irvine, w. M., Goldsmith, P. F., and Hjalmarsen, Å. 1987, in *Interstellar Processes*, eds. D. J. Hollenbach and H. A. Thronson Jr., (Dordrecht: Reidel), 561.
- Jacq, 'T., Walmsley, C. M., Baudry, A., Mauersberger, R., & Jewell, P. R. 1990, *A&A*, 228, 447.
- Kerr, T. H., Adamson, A. J., & Whittet, D. C. B. 1993, *MNRAS*, 262, 1047.
- Langer, W. D., & Graedel, 'T. E. 1989, *ApJS*, 69, 241.
- Langer, w. D., Wilson, il., W., Goldsmith, P. F., & Beichman, C. A. 1989, *ApJ*, 337, 355.
- Le Bourlot, J. 1991, *A&A*, 242, 235.
- Leger, A., Jura, h4., & Omont, A. 1985, *A&A*, 144, 147.
- Leitch-Devlin, M. A., & Williams, D. A. 1985, *MNRAS*, 213, 295.
- Leung, C. M., Herbst, E., & Huebner, W. P. 1984, *ApJS*, 56, 231.
- Luine, J. A., & Dunn, G. }1., *ApJ*, 299, L67

- Marquette, J. B., Rowe, B. R., Dupeyrat, Ronoff, G. 1985, *A&A*, 147, 115.
- Marquette, J. B., Rebrion, C., & Rowe B. R. 1988, *J. Chem. Phys.*, 89, 2041.
- Mezger, P. G., Wink, J. P., & Zylka, R. 1990, *A&A*, 228, 95.
- Meixner, M., Laas, M. R., Tielens, A. G. G. M., Prickson, E. F., & Werner, M. W. 1992, *A&J*, 390, 499.
- Millar, T. J., & Precman, A. 1984, *MNRAS*, 207, 405.
- Millar, T. J., Rawlings, J. M. G., Bennett, A., Brown, P. D., & Charney, S. B. 1999, *A&AS*, 87, 585.
- Mundy, L. G., Scoville, N. Z., Bath, L. A., Masson, C. R., & Woody, J. R. 1986 *ApJ*, 304, L51
- Olano, C. A., Walmsley, C. M., & Wilson, T. L. 1988, *A&A*, 196, 194
- Planbeck, R. C., & Wright, M. C. H. 1987, *ApJ*, 247, 187.
- Sandford, S. A., & Allamandola 1988, *Icarus*, 76, 20
- Sandford, S. A., Allamandola, L. J., Tielens, A. G. G. M., & Valero, G. J. 1988, 329, 498.
- Sandford, S. A., & Allamandola 1990, *Icarus*, 87, 188.
- Sandford, S. A., & Allamandola, L. J. 1993, *ApJ*, 409, L65.
- Savage, B. D., Gardelli, J. A., & Sofia, U. J. 1992, *ApJ*, 401, 706.
- Schutte, W. A., & Greenberg, J. M. 1991, 244, 90.
- Sodroski, T. J., Bennett, C., Boggess, N., Dwek, E., Franz, J., Hauser, M. G., Kelsal T., Moseley, S. H., Odgard N., Silverberg, R. F., and Weiland, J. L. 1994, *ApJ* in

)]”(ss.

Smith, R. G., Sellgren, K., & Brooke, T. Y. 1993, MNRAS, 263, 749.

Snell, R. L., Heyer, M., & Schloerb, F. P. 1989, ApJ, 337, 739.

Spitzer, L. Jr. 1978, in Physical Processes in the Interstellar Medium, (New York: Wiley).

Stacey, G. J., Jaffe, D. T., Geis, N., Harris, A. L., Poglitsch, A., Stutzki, J., & Townes, C. H. 1993, ApJ, 404, 219

Stutzki, J., Stacey, G. J., Genzel, R., Harris, A. L., Jaffe, D. T., & Lugten, J. B. 1988, ApJ, 332, 379

Tielens, A. G. G. M., & Hagen, W. 1982, A&A, 114, 245.

Tielens, A. G. G. M., & Hollenbach, D. 1985, ApJ, 291, 747

Tielens, A. G. G. M., & Allamandola, L. J., in Interstellar Processes, eds. D. J. Hollenbach & H. A. Thronson, (Dordrecht: D. Reidel), 397.

Tielens, A. G. G. M., Tokunaga, A. T., Geballe, T. R., & Bass, P. 1991, ApJ, 381, 181.

Turner, B. E. 1989, Space Science Reviews, 51, 235.

Turner, B. E. 1990, ApJ, 362, 129.

van Dishoeck, E. F., & Black, J. H. 1988, ApJ, 334, 771.

van Dishoeck, E. F., Blake, G. A., Draine, B. T., & Lunine, J. I. 1993, in Protostars and Planets III, eds. E. H. Levy & J. I. Lunine, (University of Arizona Press: Tucson).

Vialla, Y. P. 1986, A&AS, 64, 391.

Watson, W. D., & Salpeter, E. E. 1972, ApJ, 174, 321.

- Watson, W. D. 1975, in *Atomic and Molecular Physics and the Interstellar Matter*, Les Houches Summer School, eds. R. Balian, P. Encrenaz, & J. Lequeux, (North Holland: Amsterdam), 177.
- Whittet, D. C. B., Bode, M. F., Longmore, A. J., Adamson, A. J., McFadzean, A. D., Aitken, D. K., & Roche, R. F., 1988, *MNRAS*, 233, 321.
- Whittet, D. C. B., Adamson, A. J., Duley, W. W., Geballe, T. R., & McFadzean, A. D. 1989, *MNRAS*, 241, 707.
- Whittet, D. C. B. 1993, in *Dust and Chemistry in Astronomy*, eds. T. J. Millar & D. A. Williams, (Bristol: Institute of Physics), 9.
- Williams, D. A. 1968, *ApJ*, 151, 935.
- Williams, D. A., Hartquist, T. W., & Whittet, D. C. 1992, *MNRAS*, 258, 599.
- Williams, D. A. 1993, in *Dust and Chemistry in Astronomy*, eds. T. J. Millar & D. A. Williams, (Institute of Physics Publishing: Bristol), 143.
- Willacy, K., & Williams, D. A. 1993, *MNRAS*, 260, 635.
- Yee, J. H., Lepp, S., & Dalgarno, A. 1987, *MNRAS*, 227, 461.

Figure Captions

Fig. 1.- Time evolution of gas phase and grain surface abundances for major reservoirs of carbon, oxygen, and nitrogen (abundances are relative to H_2). The physical conditions are for the standard model but thermal evaporation off of 10 K dust grains is the only desorption process.

Fig. 2.- Time evolution of gas phase and grain surface abundances (abundances are relative to H_2) for major reservoirs of carbon, oxygen, and nitrogen for the standard model at $\tau_V = 10.3$ mag (upper panel) and $\tau_V = 2.1$ mag (lower panel).

Fig. 3.- Time evolution of gas phase and grain surface abundances (abundances are relative to H_2) for trace carbon and oxygen bearing species for the standard model at $\tau_V = 10.3$ mag (upper panel) and $\tau_V = 2.1$ mag (lower panel).

Fig. 4.- Time evolution of gas phase and grain surface abundances (abundances are relative to H_2) for trace nitrogen bearing species for the standard model at $\tau_V = 10.3$ mag (upper panel) and $\tau_V = 2.1$ mag (lower panel).

Fig. 5.- Profile of gas phase and grain surface abundances (abundances are relative to H_2) against depth for major carbon, oxygen, and nitrogen bearing species. The profiles are for the standard model at 10^5 yr (upper panel) and 10^7 yr (lower panel).

Fig. 6.- Same as Fig. 5 except for trace carbon and oxygen compounds.

Fig. 7.- Same as Fig. 5 except for trace nitrogen bearing molecules.

Fig. 8.- Time evolution of gas and grain mantle abundances (abundances relative to H_2) for selected species for the star "turn on" model. The physical conditions are the same as the standard model except $T_{dust} = 25$ K. The initial conditions for this figure are the abundances from the standard model at 10^7 yr.

Fig. 9.- Same as Fig. 10 except $T_{dust} = 30$ K.

Fig. 10.- Depletion from the gas phase for selected species as a function of density at 10^7 yr for $T_{dust} = 10$ K, $\chi = 1.0$, $T_{gas} = 20$ K. $n_{X(surface)}/n_{X(gas+surface)}$ is defined as 1 = 100 percent depletion.

Fig. 11.- Depletion of CO from the gas phase at 10^7 yr as a function of molecular hydrogen density for three different binding surfaces: CO bonding with a pure CO surface, CO bonding with a SiO_2 surface, and CO bonding onto a water ice surface. $n_{CO(surface)}/n_{CO(gas+surface)}$ is defined as 1 = 100 percent depletion.

Fig. 12.- Profile distribution of gas and grain surface abundances (abundances relative to H_2) against depth for select species at 10^7 yr. Physical conditions and desorption processes are the same as the standard model except $T_{dust} = 20$ K (upper panel) and $T_{dust} = 30$ K (lower panel).

Fig. 13.- Profile distribution of gas and grain surface abundances (abundances relative to H_2) against depth for select species at 10^7 yr. Physical conditions and desorption processes are the same as the standard model except for an enhanced radiation field, $\chi = 100$.

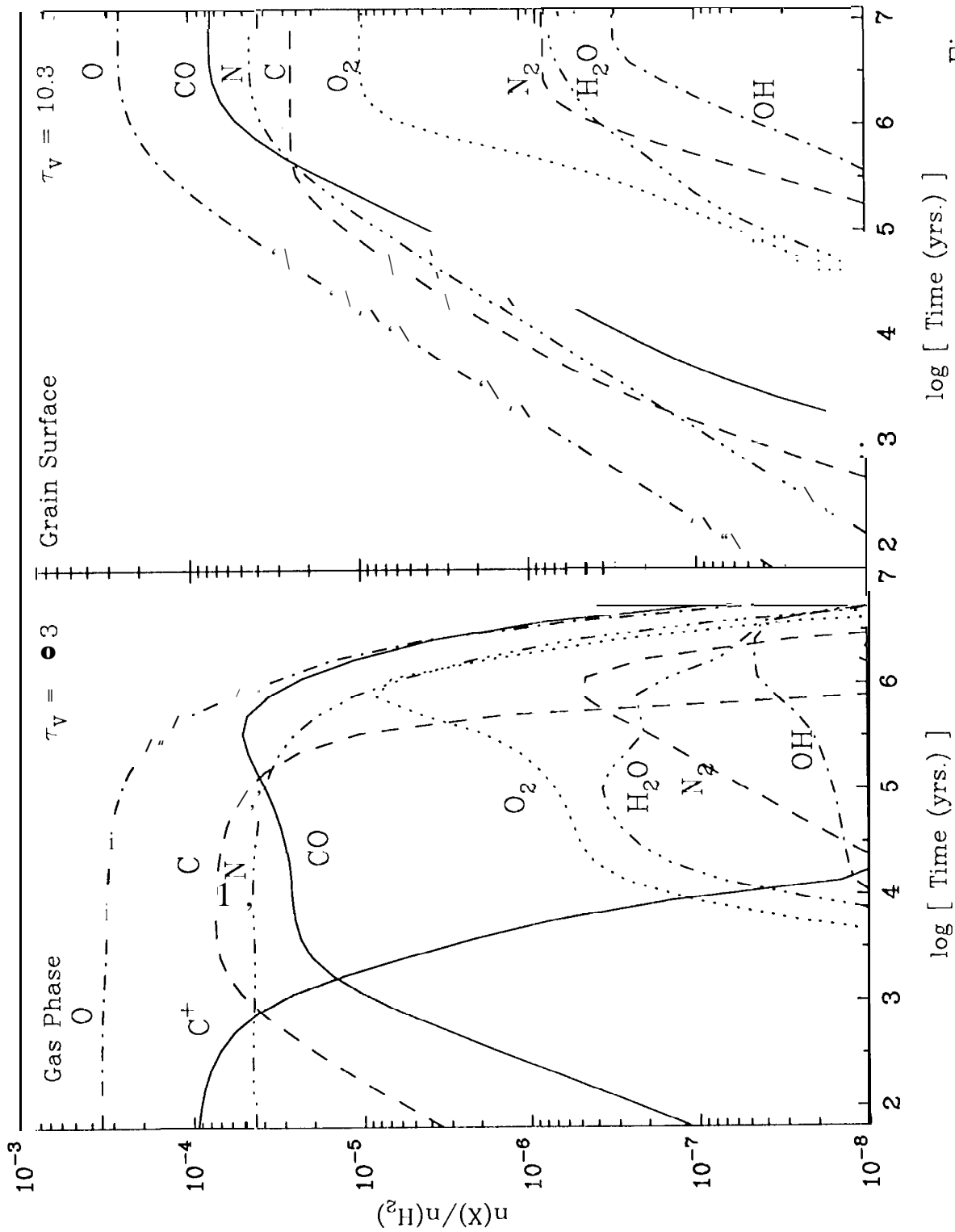


Figure 1

Figure 2

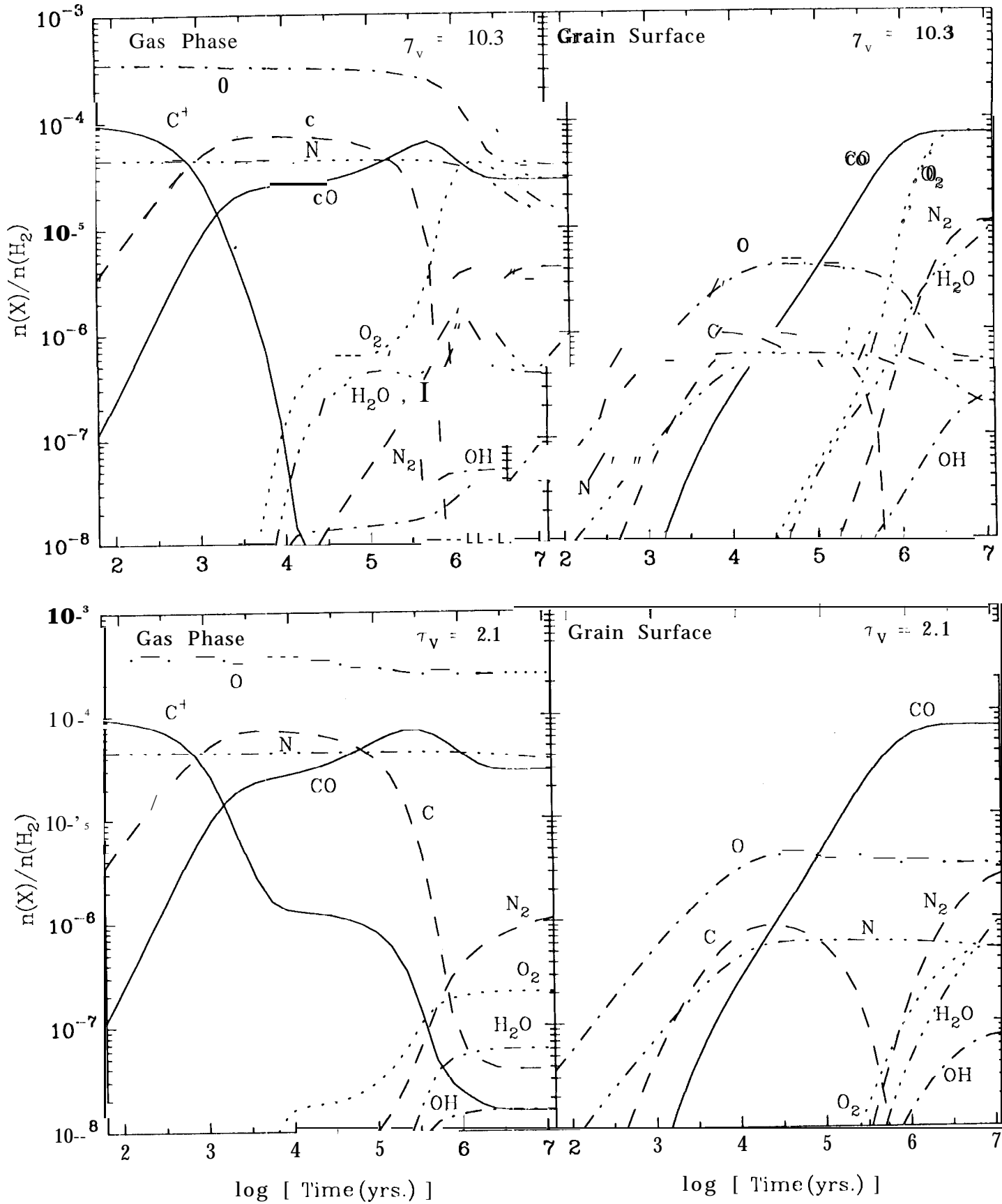


Figure 3

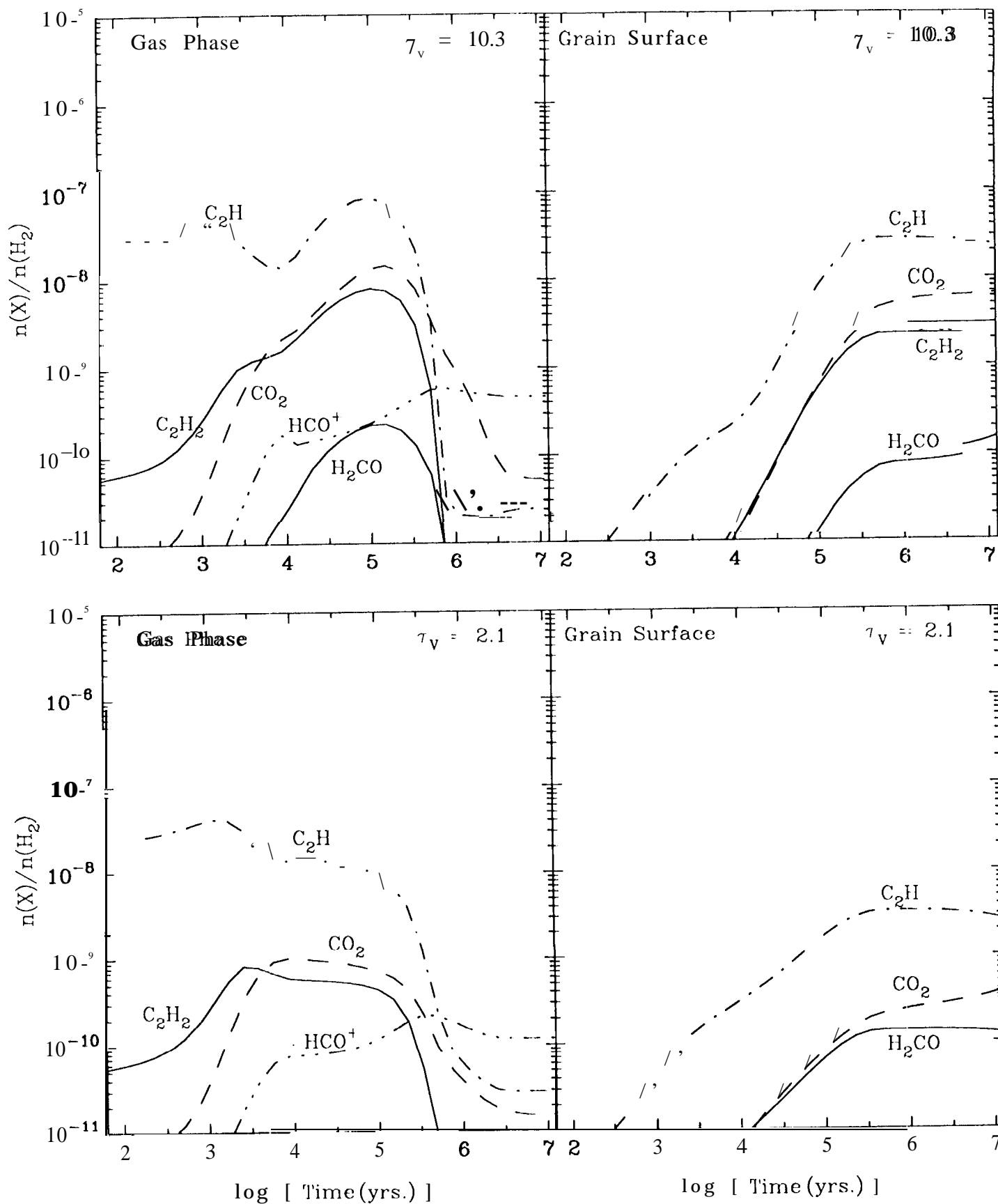


Figure 4

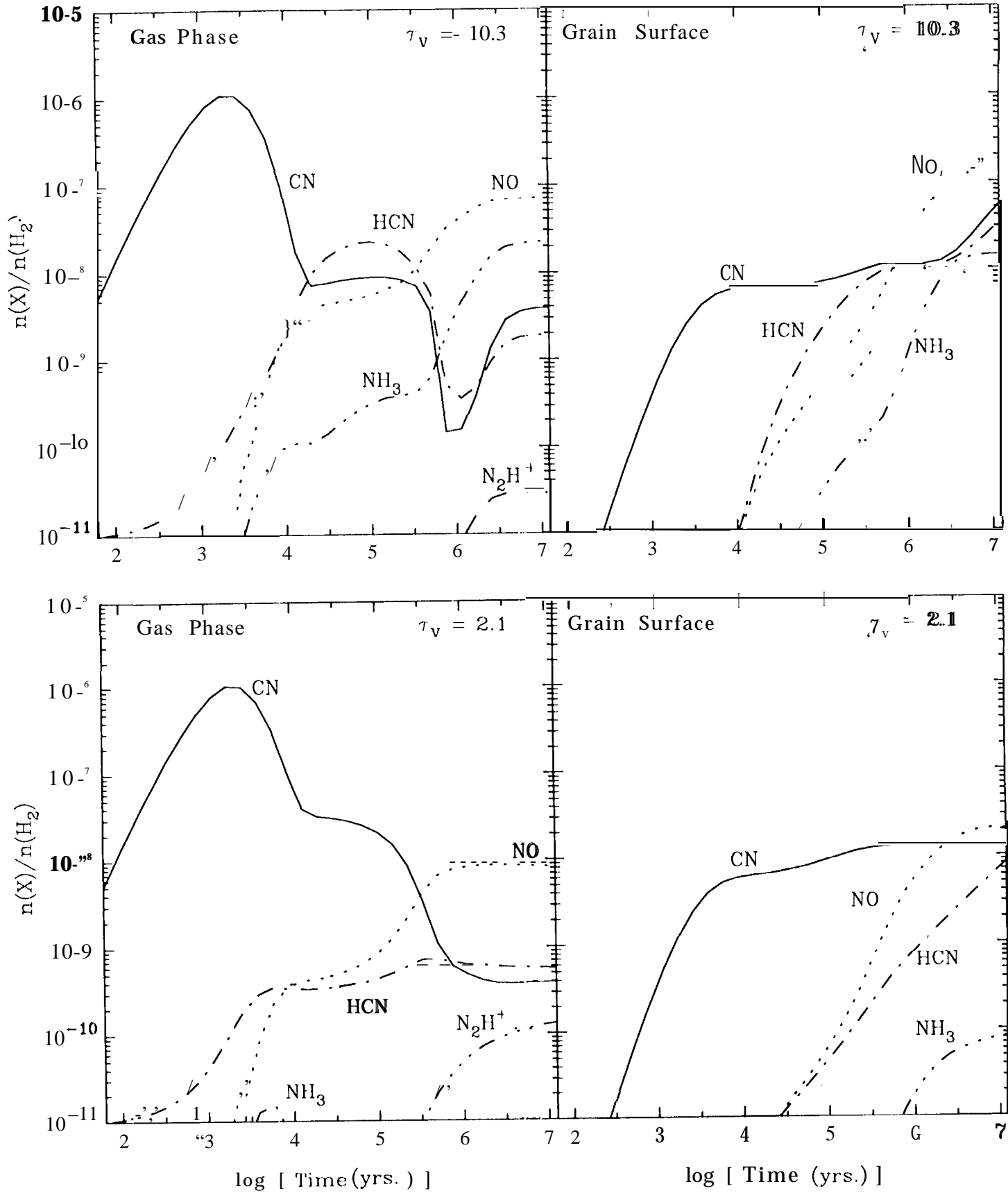


Figure 5

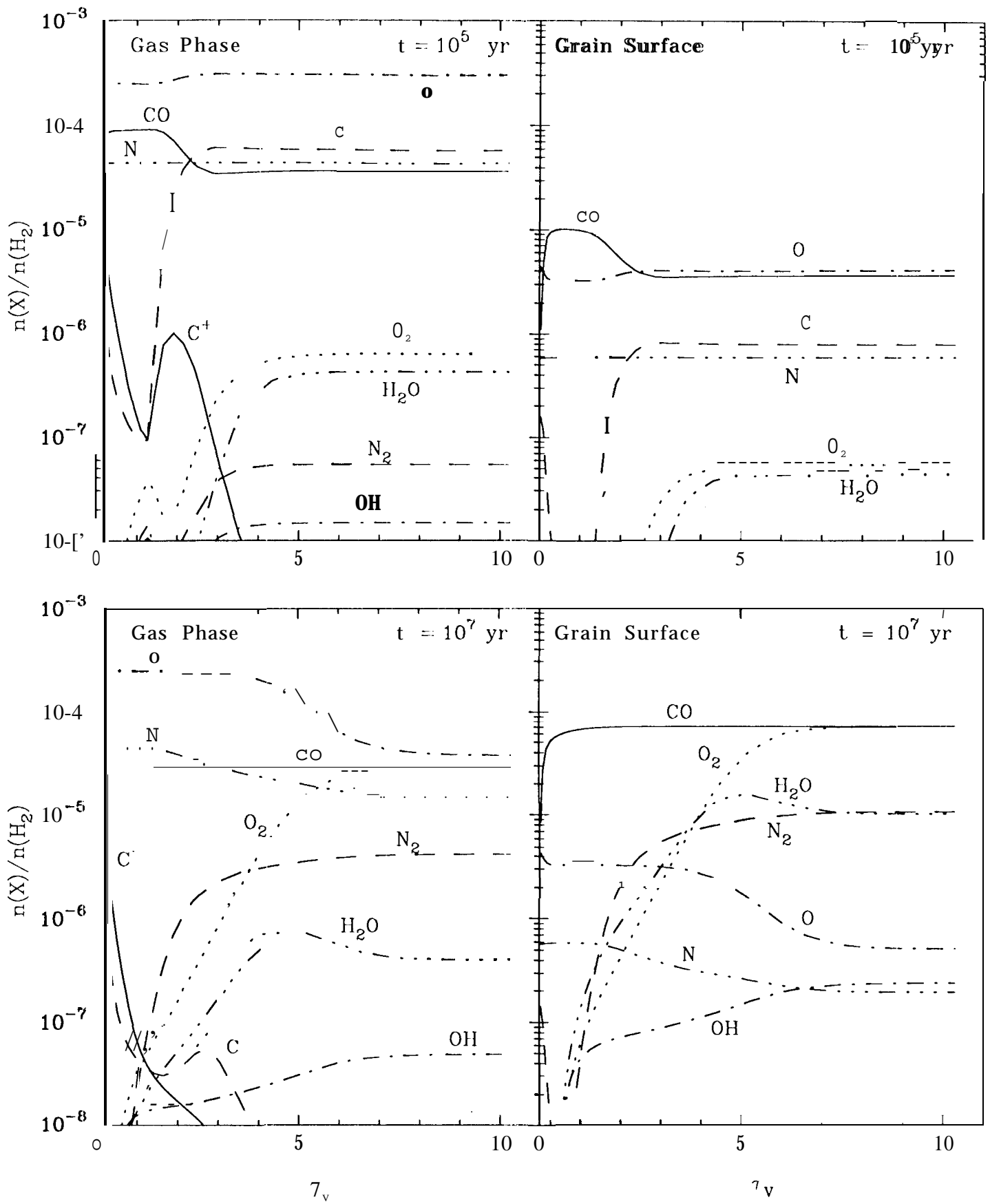


Figure 6

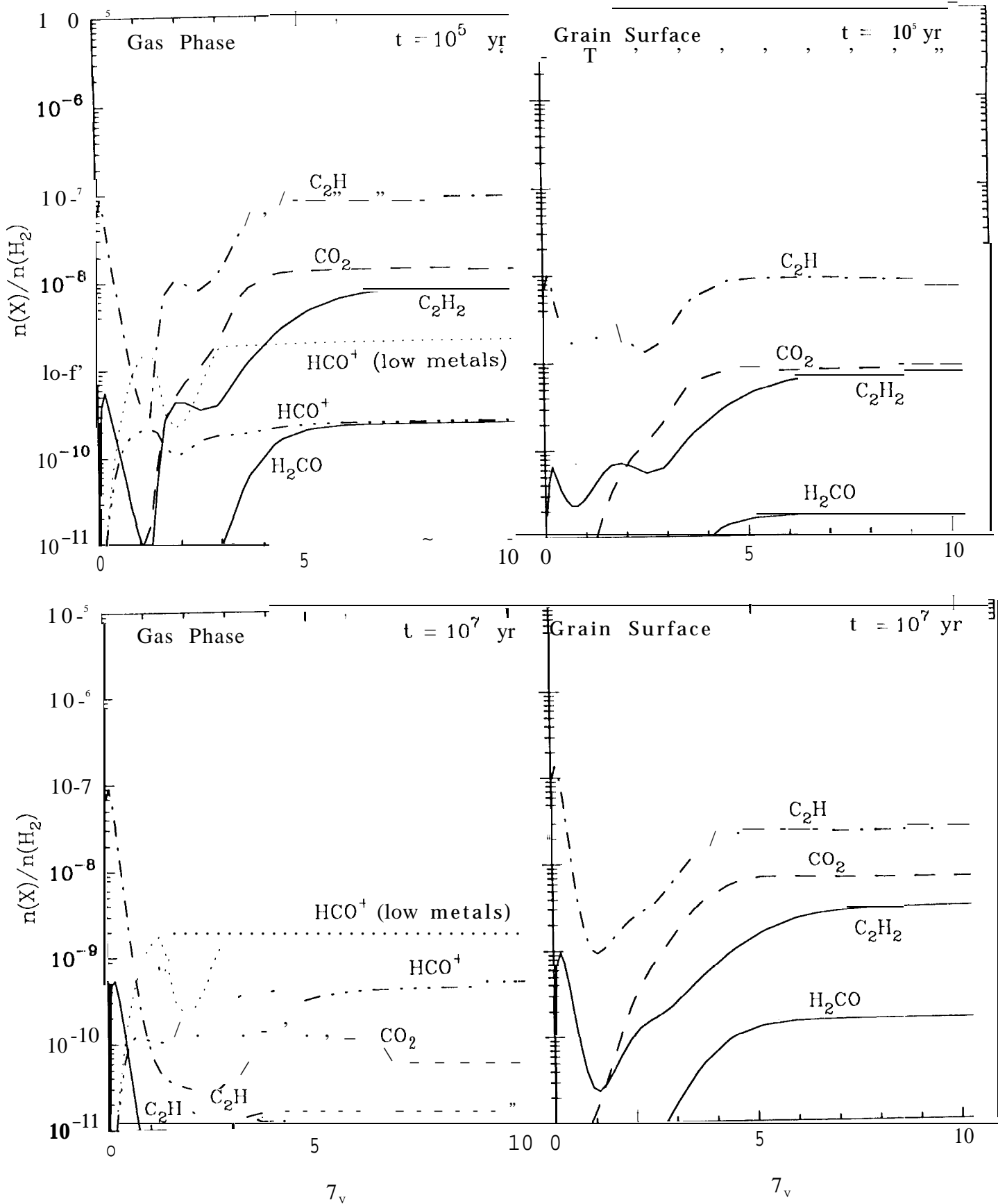


Figure 7

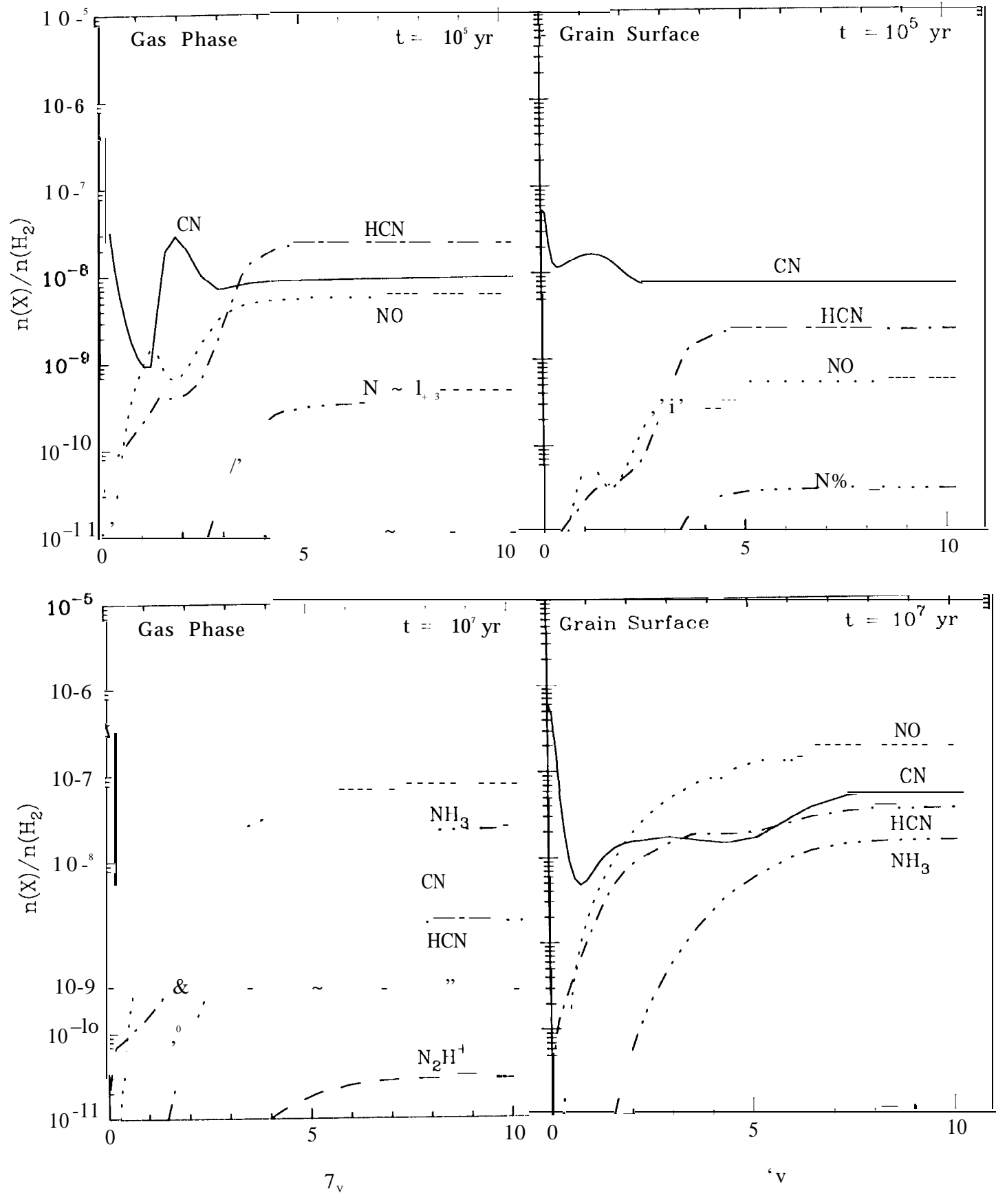


Figure 8

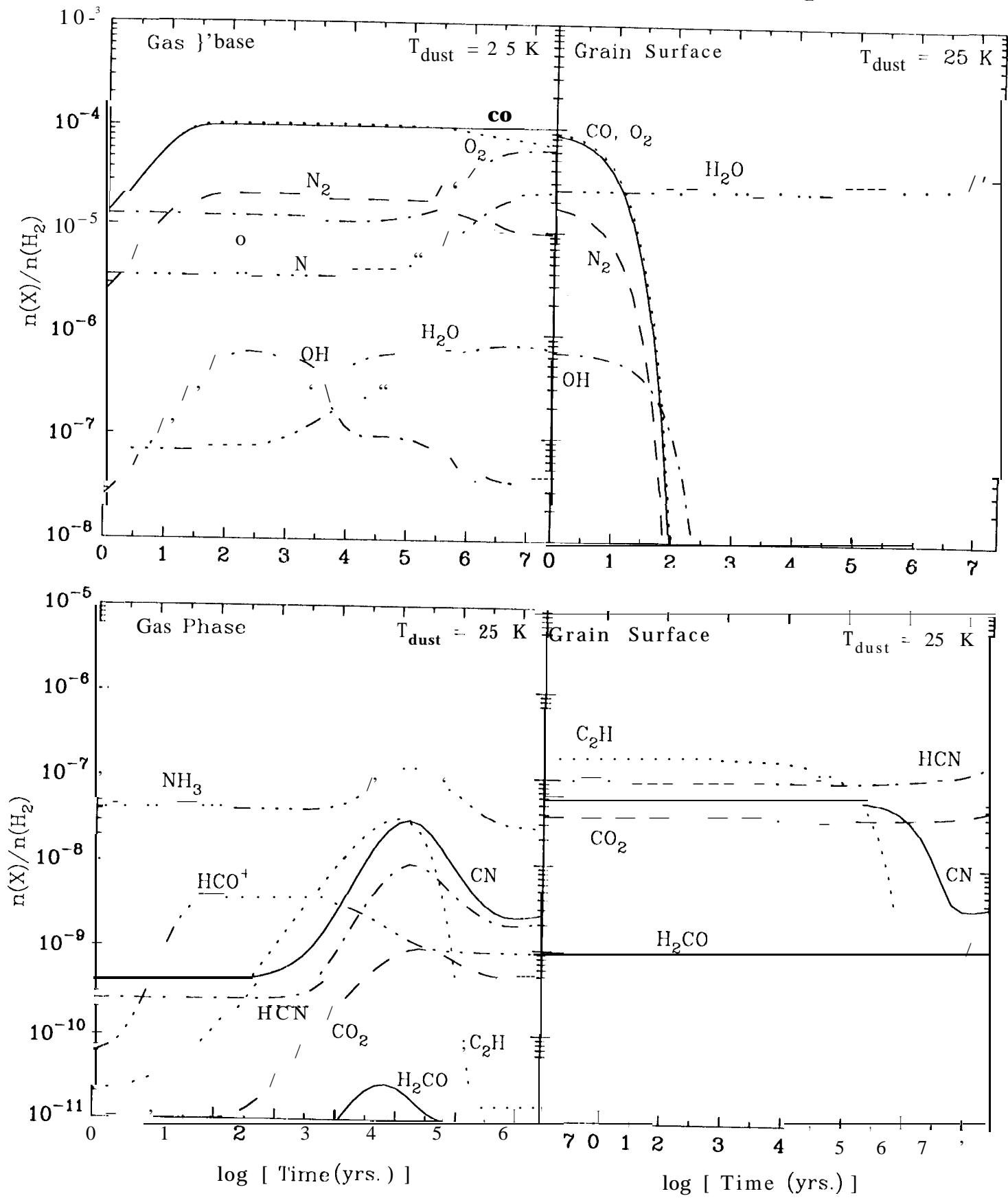
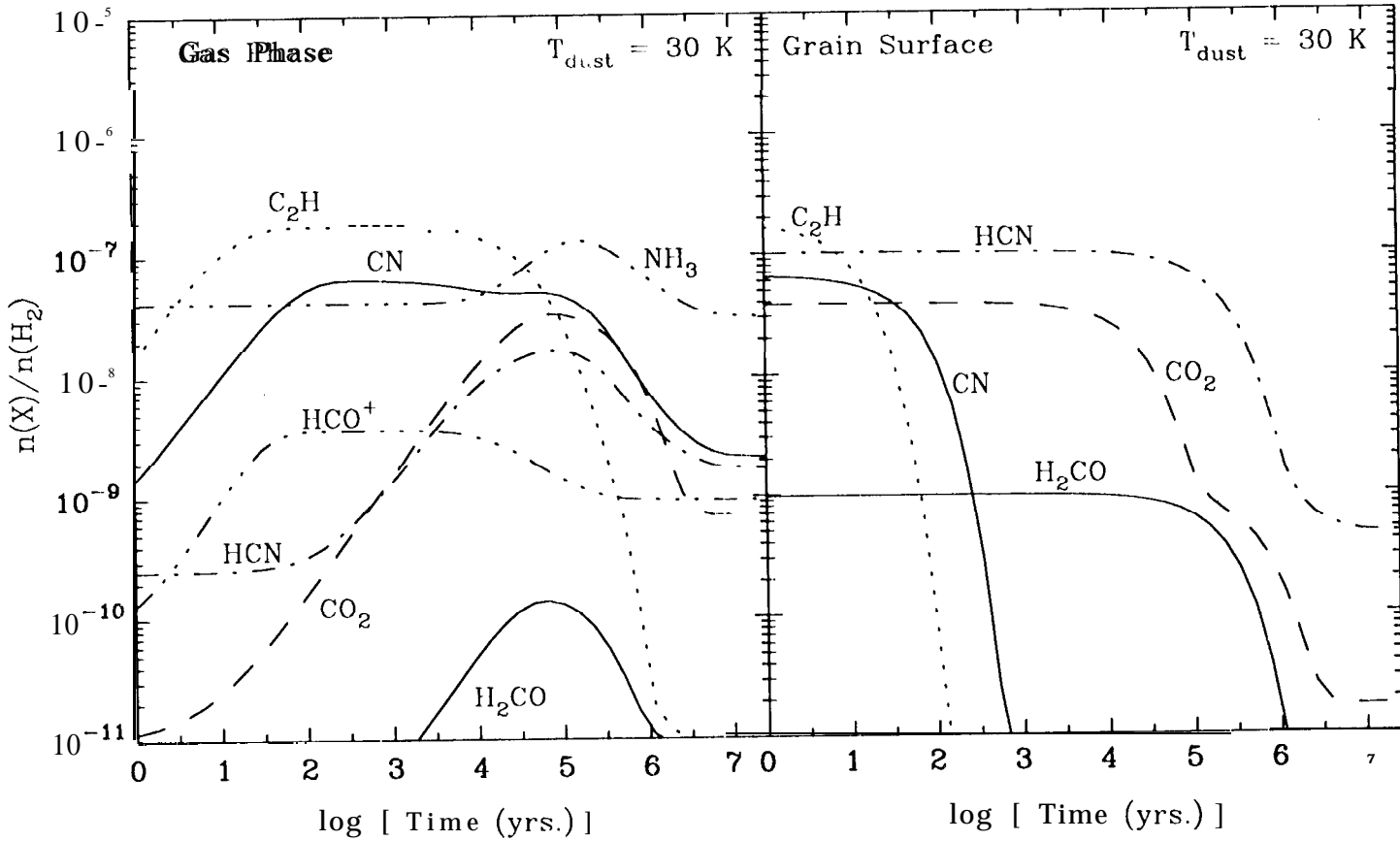
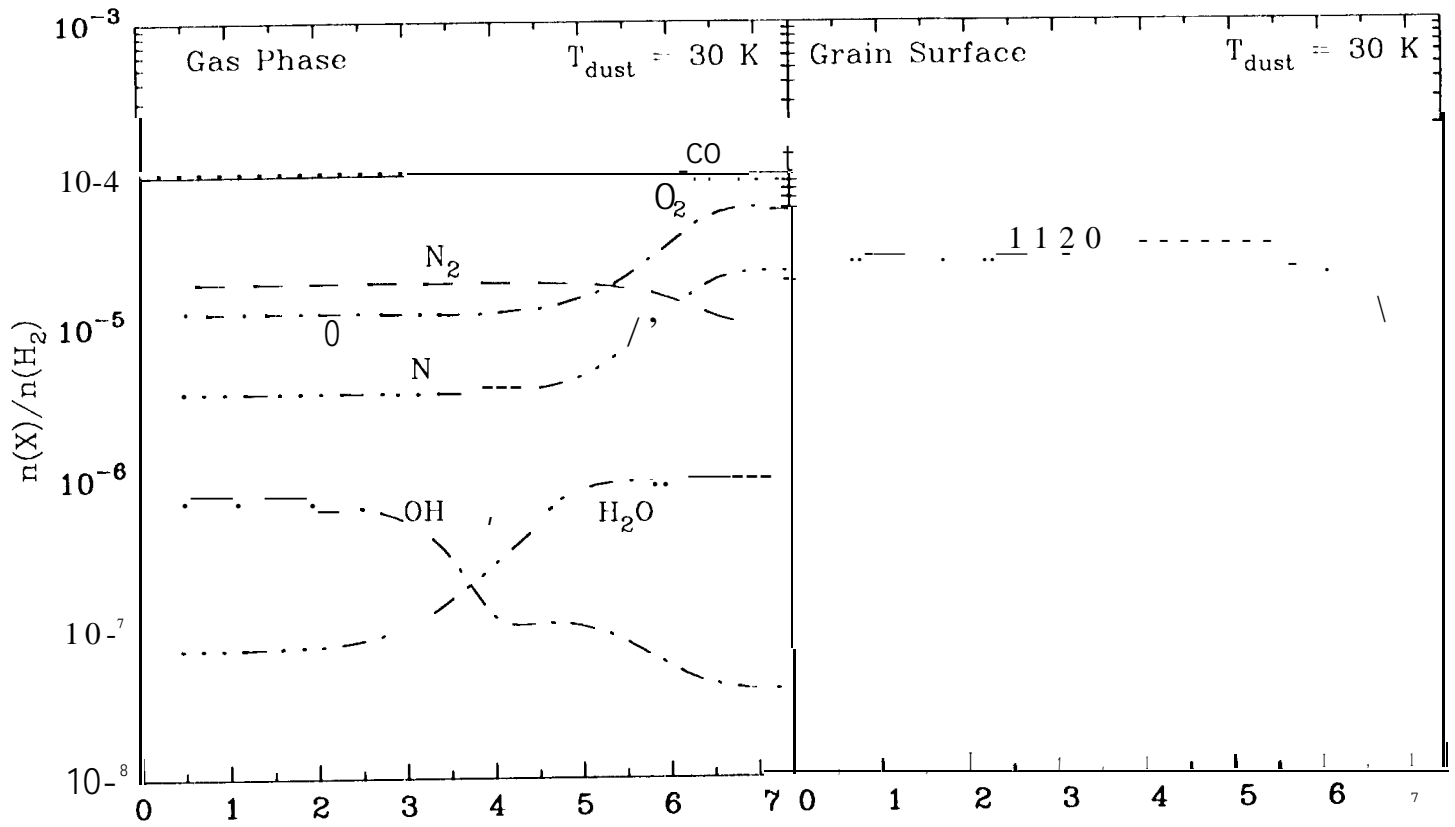


Figure 9



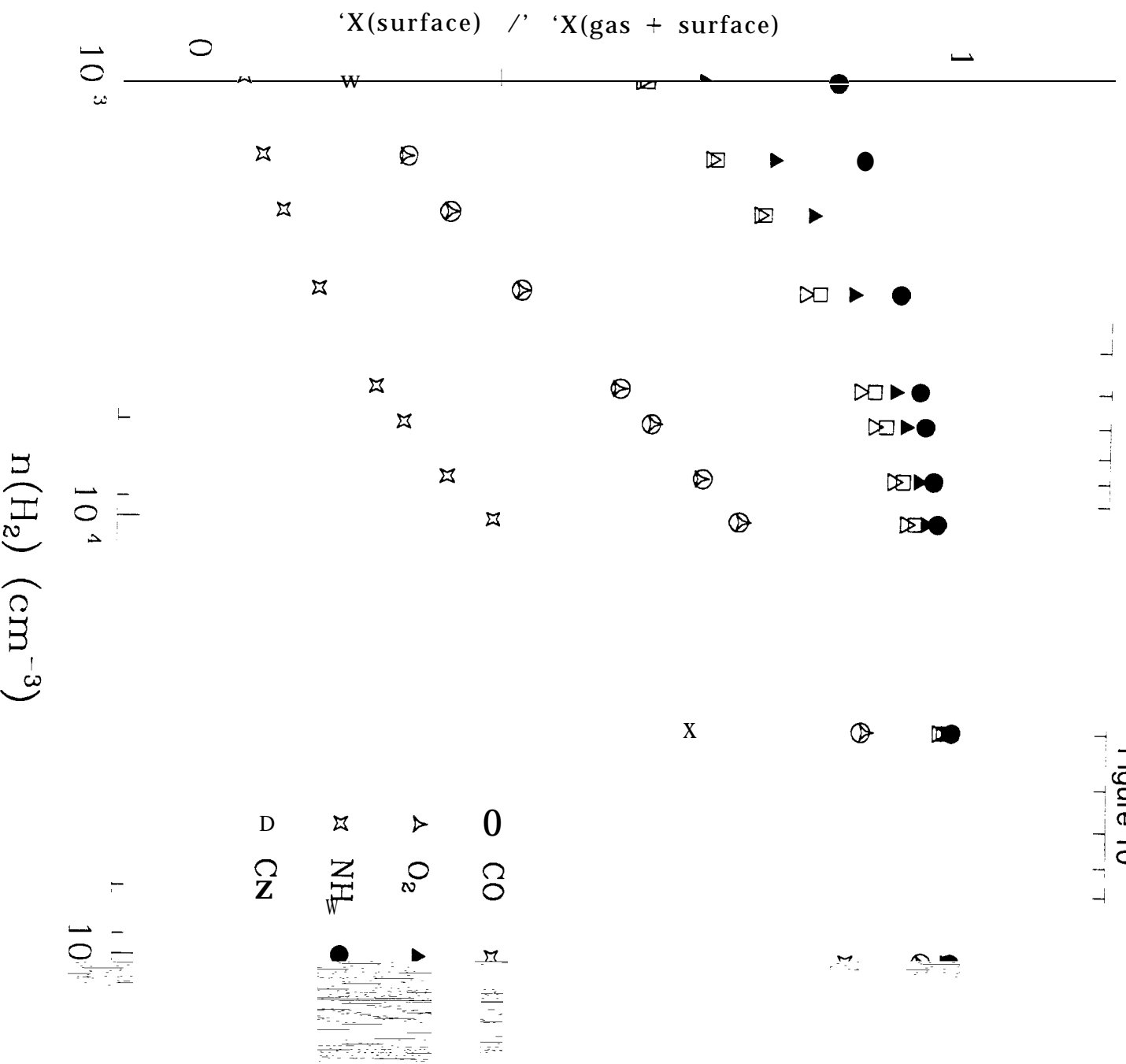


Figure 10

Figure 11

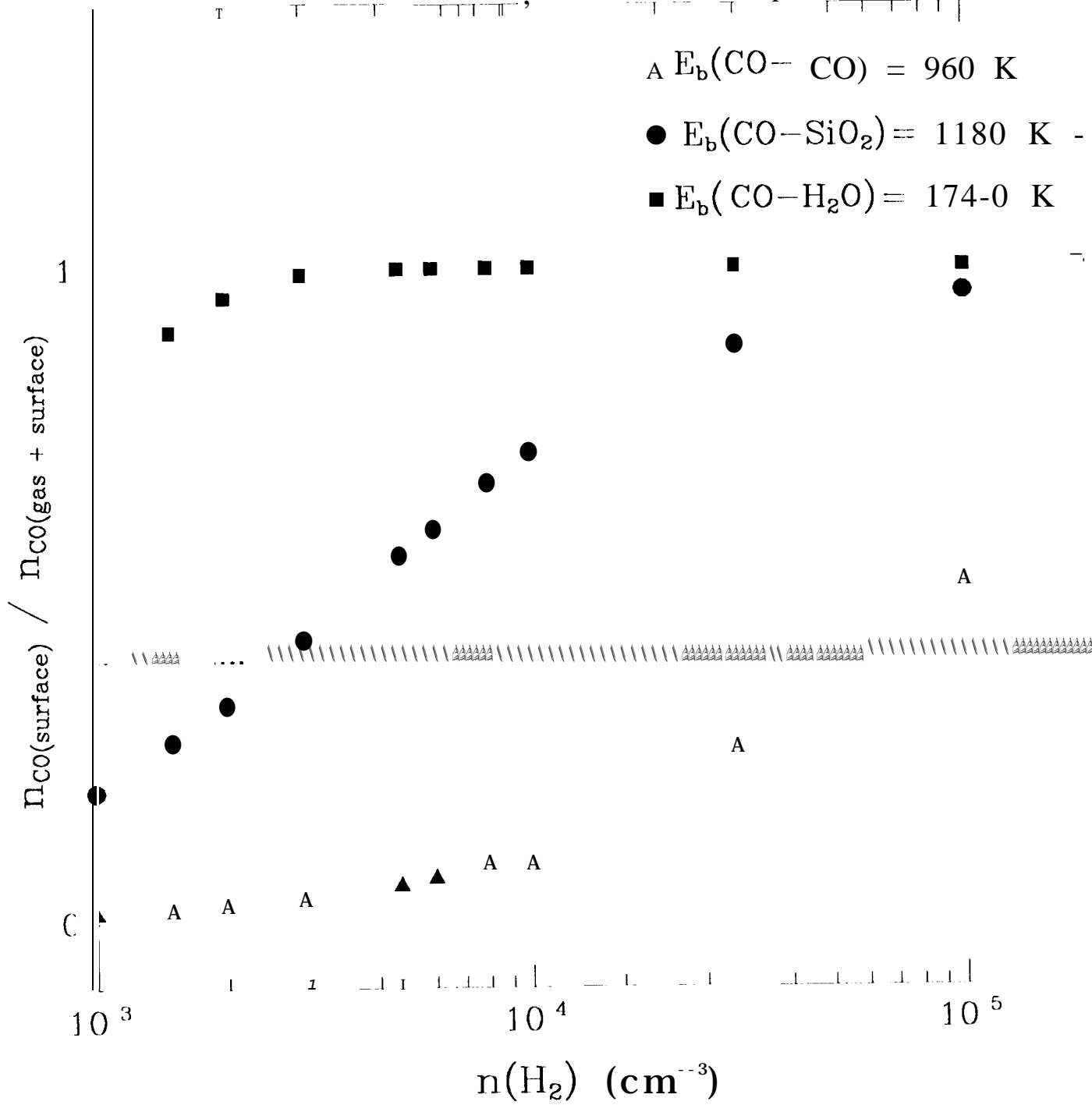


Figure 12

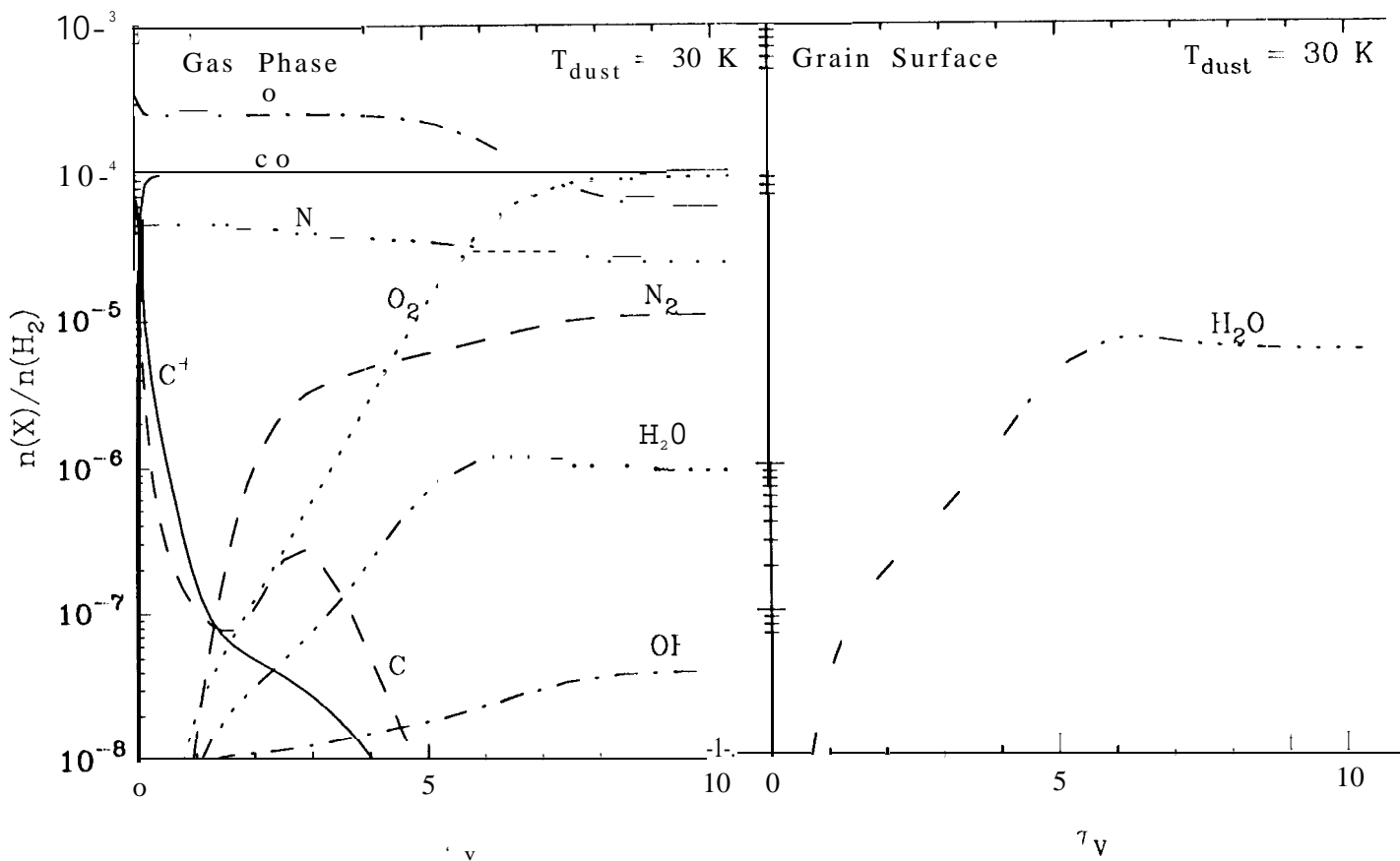
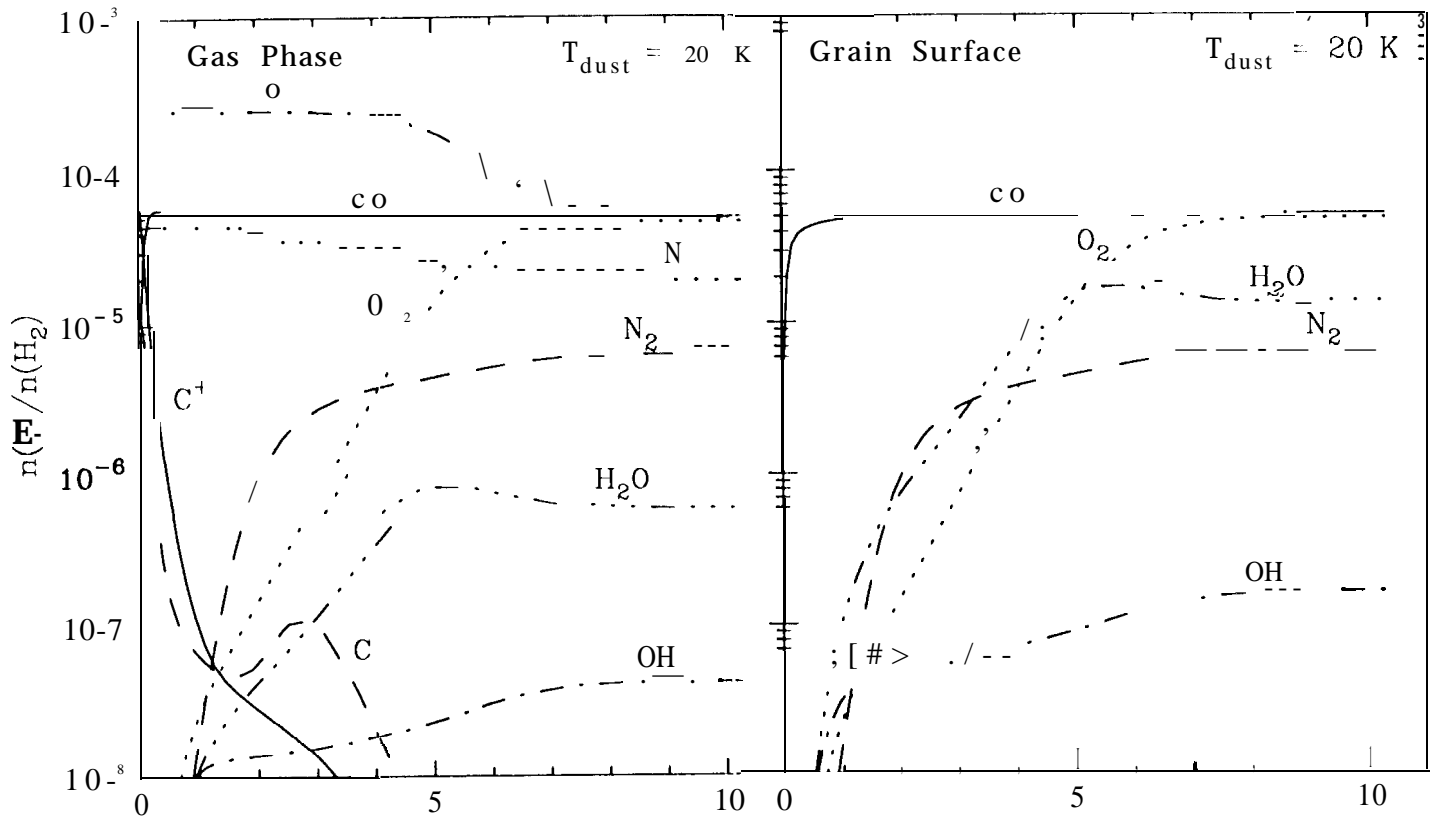


Figure 13

